TEKNILLINEN TIEDEKUNTA

CRASH TEST SIMULATION AND OPTIMIZATION OF ROAD SIDE BARRIER

Rainer Leikkonen

Ohjaaja: Hannu Koivurova

KONETEKNIIKAN TUTKINTO-OHJELMA

Diplomityö 2019

TIIVISTELMÄ

Maantiekaiteen törmäyssimulointi ja rakenteen optimointi

Rainer Leikkonen

Oulun yliopisto, Konetekniikan tutkinto-ohjelma

Diplomityö 2019, 70 s.

Työn ohjaaja yliopistolla: Hannu Koivurova

Maanteiden suojakaiteilta vaadittavat ominaisuudet ovat ristiriitaisia. Kaiteen tulee olla riittävän jäykkä estääkseen törmäyksessä ajoneuvoa ajautumasta kauas ulos ajoradalta. Samalla kaiteen on myös joustettava, jotta törmäyksessä ajoneuvon matkustajiin kohdistuvat kiihtyvyydet eivät nouse vaarallisen suuriksi. Tasapainon löytämiseksi näiden kahden ominaisuuden välille voi vaatia monta iteraatiota kaiteen rakenteesta, eikä törmäyskokeen järjestäminen jokaista iteraatiota varten ole mielekästä. Suunnittelijan työtuntien vähentämiseksi eri kaidegeometrioiden vertailu olisi edullista automatisoida.

Tämän diplomityön tavoitteena on luoda simulaatiomalli, joka kuvaa riittävän tarkasti törmäyksen fyysiset tapahtumat ja jota voidaan jatkossa käyttää avuksi uusien kaiteiden suunnittelussa. Kun mallin katsotaan olevan riittävän tarkka, se voidaan liittää optimointirutiiniin, joka hakee kaiteen rakenteelle parhaat mahdolliset mitat annettujen rajoitteiden puitteissa.

Törmäyskokeesta onnistuttiin luomaan tyydyttävän tarkka simulaatiomalli, joka voitiin liittää optimointirutiiniin. Optimointirutiinin avulla pystyttiin automaattisesti selvittämään uuden kaidekokoonpanon tolppien profiilin mitat mallin tarkkuuden puitteissa mahdollisimman hyväksi. Mallia voidaan käyttää uudenlaisten kaidegeometrioiden arvioimiseen ja käytettyä optimointirutiinia voitaisiin soveltaa myös muunlaisiin monimutkaisiin simulaatioihin.

Asiasanat: Törmäyssimulaatio, Optimointi, Tiekaide

ABSTRACT

Crash test simulation and optimization of road side barrier

Rainer Leikkonen

University of Oulu, Degree Programme of Mechanical Engineering

Master's thesis 2019, 70 p.

Supervisor at the university: Hannu Koivurova

The performance requirements for roadside barriers are partly contradictory. The barrier should be stiff enough to contain the car during crash. At the same time the barrier should be flexible enough that the accelerations experienced by the passengers are not dangerously high. To achieve balance between the stiffness and flexibility might require several iterations of the barrier geometry. Performing a full-scale crash test for each iteration is not desirable. Also, to reduce the man hours required for the development of a new barrier the process of iterating different barrier geometries should be automatized.

The goal of this thesis is to develop a finite element model that can present the physical events of a car crashing into a roadside barrier with reasonable accuracy and can therefore be used in the development of new barriers. Once the model is accurate enough it can be coupled with a optimization routine to search for the optimal dimensions of the barrier geometry.

A reasonably accurate simulation model was successfully developed and paired with an optimization routine. With the optimization routine optimal dimensions for the geometry of the posts profile were successfully iterated. The model can be used for the development of new barriers and the optimization routine could be implemented to other similarly challenging simulations.

Keywords: Crash test simulation, Optimization, Roadside barrier

PREFACE

This thesis aims to explore the possibility of combining an optimization routine into an explicit finite element simulation. The simulation in question is a crash simulation of a car into a roadside barrier. SSAB ordered a development of a roadside safety barrier crash simulation model and the development of a new barrier. The viability of coupling optimization routine into an explicit simulation is evaluated in development of the new barrier. The work was done between May of 2018 and January of 2019.

I would like to thank my colleagues at Elomatic Oy for their help in the thesis and my superior Leo Siipola for arranging the subject for the thesis and guidance during the work. I would also like to thank Anssi Hyvärinen from SSAB for providing the necessary information to complete the thesis and Hannu Koivurova at the University for supervising this work. Finally I would like to thank my girlfriend Heta Vepsäläinen for proofreading the thesis and support during my studies and my mother and my late father for putting a strong emphasis on my studies and supporting me throughout my education.

Tampere, 09.01.2019

Rainer Leikkonen

TABLE OF CONTENTS

SYMBOLS AND ABBREVIATIONS

A_x, A_y, A_z	recorded components of vehicle acceleration
$\bar{A}_x$, $\bar{A}_y$, $\bar{A}_z$	filtered components of vehicle acceleration
$\boldsymbol{A}_e$	coefficient matrix for linear equality system
$\boldsymbol{A}_i$	coefficient matrix for linear inequality system
$\boldsymbol{a}_L$	vector of lower bounds for linear inequality system
$\boldsymbol{a}_U$	vector of upper bounds for linear inequality system
$\boldsymbol{a}_t$	vector of target values for linear equality system
C_{XY}	moving ground reference frame
C_{xy}	vehicle reference frame
c_d	wave speed of material
c_e	wave speed in an element
D_x, D_y	flail distances
D_m	dynamic deflection
E	Young's modulus
E_A	artificial strain energy
E_{CD}	dissipated energy though viscoelasticity or creep
E_{CW}	work done by constraint penalties
E_{DC}	dissipated energy through distortion control
E_{DMD}	dissipated energy through damage
E_E	elastic strain energy
E_{FC}	fluid cavity energy
E_{FD}	frictional dissipated energy
E_{HF}	external energy through external fluxes
E_I	internal energy
E_{IHE}	internal heat energy
E_{KE}	kinetic energy
E_{MW}	work done by propelling added mass
E_P	dissipated energy through inelastic prosesses
E_{PW}	work done by contact penalties
E_{total}	sum of energies
E_V	viscous energy dissipated
E_W	work done by external applied loads

F	internal and applied external element forces
f	objective function
$\boldsymbol{g}$	nonlinear inequality constraint vector
$\boldsymbol{g}_L$	vector of lower bounds of inequality constraints
$\boldsymbol{g}_U$	vector of upper bounds of inequality constraints
$\boldsymbol{h}$	nonlinear equality constraint vector
$\boldsymbol{h_t}$	vector of target values of nonlinear equality constraints
l_e	characteristic length of an element
M	nodal mass matrix
u	nodal displacement
$\dot{u}$	nodal velocity
$\ddot{u}$	nodal acceleration
t	time
Δt	time step
Δt_{crit}	critical time step
VI_m	vehicle intrusion
W_m	working width
W_n	normalized working width
X_b	head position in ground coordinates
$\dot{X}_b$	head velocity in ground coordinates
X_C	vehicle position in ground coordinates
$\dot{X}_C$	vehicle velocity in ground coordinates
$\ddot{X}_C$	vehicle acceleration in ground coordinates
x	denotes longitudinal vehicle axis
$\boldsymbol{x}$	design variable vector
x_b	head displacement in vehicle reference frame
$\dot{x}_b$	head velocity in vehicle reference frame
$\boldsymbol{x}_L$	vector of lower bounds of the design variables
$\boldsymbol{x}_U$	vector of upper bounds of the design variables
x_0	initial distance of head from C_{XY}
Y_b	head position in ground coordinates
$\dot{Y}_b$	head velocity in ground coordinates
Y_C	vehicle position in ground coordinates
$\dot{Y}_C$	vehicle velocity in ground coordinates

$\ddot{Y}_C$	vehicle acceleration in ground coordinates
y	denotes transverse vehicle axis
y_b	head displacement in vehicle reference frame
$\dot{y}_b$	head velocity in vehicle reference frame
y_0	initial distance of head from C_{XY}
z	denotes vertical vehicle axis
α	reduction factor for destabilizing effects of nonlinearities
ρ	density
Ψ	yaw
$\dot{\Psi}$	rate of yaw
ω_e	maximum frequency of a element
ω_{max}	maximum frequency of a system
ASI	Acceleration severity index
THIV	Theoretical index of head velocity

1 INTRODUCTION

Accidents involving vehicles running of roads and hitting various impediments, such as trees, walls or vehicles travelling into the other direction are a major concern worldwide. According to National Cooperative Highway Research Program (1997) approximately one third of all traffic fatalities on US highways are caused by such crashes (Teng et al. 2016, p. 565). On dangerous sections of the road roadside barriers can be installed to prevent the vehicle from leaving the road. Roadside barriers absorb the impact energy and redirect the vehicle back on road. Installation of roadside barriers can have major effect on the amount of crashes that cause injuries. Data collected by The European Union Road Federation has shown that on some roads with high accident frequency the installation of roadside barriers has lowered the number of accidents causing injuries by up to 91% (Teng et al. 2016, p. 565).

Development of roadside barrier is dictated by the requirements presented in European standard EN-1317. The barrier should contain the vehicle and only deform an allowable amount. At the same time the barrier should not be too stiff so that the passengers experience harmful accelerations. Achieving a balance between these two might require evaluation of performance of several potential barrier assemblies. Performing a full-scale crash tests can be expensive, so the engineer should be confident in the performance of the barrier before committing to a full-scale test. To predict the performance of the barrier the use of finite element model is common practice. However, even with the most accurate model of the crash the engineer still has to manually iterate to find a good enough geometry for the barrier. In this thesis we look into the possibility of using optimization software to reduce the iterative work done by the engineer. The goal is to produce a finite element model and couple it with optimization software to automatically find the best geometry for a roadside barrier assembly.

2 FINITE ELEMENT METHOD

Finite element method is a numerical method of finding an approximate solution to a complicated differential equation by replacing it with many algebraic equations. Often the existing mathematical tools are not enough to find the exact or even an approximate solution to most of the differential equations of practical problems. Thus, finite element method is often the only viable method to find even an approximate solution.

For structural analysis the continuum under study is divided into a finite number of elements. These elements are connected to each other at nodes which are at the end of the elements in 1D elements and corners of the elements in 2D and 3D elements. The nodes have degrees of freedom, DOF's, according to their possible translational and rotational movements in x-, y- and z-directions. From the values of the nodes DOF's the displacement of the element can be calculated and with the elements materials mechanical behaviour known the mechanical behaviour can also be determined. Performing this for every element in a structured manner provides an approximate solution for the entire continuum.

There are several commercial FEM programs available. For the simulations in this thesis Abaqus 2017 developed by Dassault systèmes has been used.

2.1 Explicit time integration

The explicit finite element method has been widely adopted for the simulation of impact problems as it handles well the nonlinearities characteristic for them. These nonlinearities include large deformation, large rotation, nonlinear material, contact etc (Wu & Lei 2012, p. 4-5). Explicit method has been used previously on various kinds of crashworthiness analysis including crash tests of roadside barriers (Ren & Vesenjak 2005, p. 967; Teng et al. 2016, p. 570). In the explicit time-integration method kinematic conditions at one time increment are used to calculate the kinematic conditions at the next increment.

The simulation problem in transient structural mechanics is of the form:

$$M\ddot{u}^{(i)} = F(t), \tag{1}$$

where M is the nodal mass matrix, $F(t)$ is the internal and applied external element forces and $\ddot{u}$ is the nodal acceleration. The superscript (i) refers to the increment number. We consider here an algorithm with a variable time increment. According to Belytschko et al. (2014, p. 330) for most practical problems this is necessary.

According to Abaqus (2017) online documentation nodal accelerations $\ddot{u}$ can be calculated out of (1) as

$$\ddot{u}^{(i)} = [M]^{-1} * F(t). \tag{2}$$

Now that the acceleration at increment (i) is known and the initial state of the problem is assumed to be known, i.e. initial nodal acceleration $\ddot{u}^0$, initial nodal velocity $\dot{u}^0$ and initial nodal displacement u^0 are known, velocities at increment $i + \Delta i/2$ can be calculated as

$$\dot{u}^{(i+\frac{1}{2})} = \dot{u}^{(i-\frac{1}{2})} + \frac{\Delta t^{(i+1)} + \Delta t^{(i)}}{2} \ddot{u}^{(i)}, \tag{3}$$

where Δt is the time step.

With (3) nodal displacements at increment $i + 1$ can be calculated using the central difference method as

$$u^{(i+1)} = \mathrm{u}^{(i)} + \Delta t^{(i+1)} \dot{u}^{(i+\frac{1}{2})}. \tag{4}$$

The use of lumped, diagonal mass matrix M makes it so that the update of nodal velocities and displacements can be done without solving any equations. This is the determining feature of explicit method: *the time integration of the discrete momentum equations does not require the solution of any equations.* (Belytschko et al. 2014, p. 332.)

2.2 Time incrementation

2.2.1 Stable time increment

The explicit method is only conditionally stable. Belytschko et al. (2014, p. 335) describes the stability of the explicit method as follows: if the length of the time step exceeds a critical value Δt_{crit}, the solution will grow without limits. The critical time step is also

called stable time step. A stable time step Δt must meet the stability condition known as the Courant condition:

$$\Delta t \leq \alpha \Delta t_{crit}, \Delta t_{crit} = \frac{2}{\omega_{max}} \leq min_e \frac{2}{\omega_e} = min_e \frac{l_e}{c_e}, \quad (5)$$

where ω_{max} is the maximum frequency of the system, ω_e is the maximum frequency of element e, l_e is a characteristic length of element e, c_e is the current wave speed in element e, and α is a reduction factor used to account for destabilizing effects of nonlinearities; taken usually in the range of $0.8 \leq \alpha \leq 0.98$.

As presented above and by Wu & Lei (2012, p. 4-5) determining the maximum frequency of the whole system is not practical due to computational cost and lack of eigen solver in the explicit code. A conservative estimate of using a critical time step based on the element with the highest frequency can be made. As can be seen in equation (5), the maximum frequency of element e can be redefined using the characteristic length of the element and the current wave speed in the element.

Wave speed in element c_e is property of its material. The wave speed c_d of material is dependent on the Young's modulus E and density ρ:

$$c_d = \sqrt{\frac{E}{\rho}}. \quad (6)$$

From (6) it can be seen that the stiffer the material the shorter the stable time step and the heavier the material the longer the stable time step. Artificially increasing the density of an element is called mass scaling and it is discussed in the next chapter.

2.2.2 Mass scaling

Artificially increasing the mass density of elements increases the stable time step which in turn decreases the computational time required for the analysis. Complex geometries may have difficult to mesh areas and end up containing few significantly smaller elements than the rest of the model. These small elements control the stable time step of the whole model. Scaling the mass of these few small elements can significantly increase the stable time step while keeping the dynamic behaviour unaffected.

When using mass scaling for transient dynamic events only few elements should be affected by it. The overall mass of the should not increase significantly as it would degrade the accuracy of the solution. (Abaqus 2017.)

2.3 Energy balance

According to Belytschko et al. (2014, p. 335), instability in a non-linear analysis can develop even when the stability condition (5) is satisfied. Belytschko et al. note that the stability condition originates from a stability analysis of the integrator for the linear equations of motion and that there are no stability theorems that cover the nonlinear phenomena characteristic for engineering problems, such as contact-impact, tearing, etc. While instability in linear problems leads to exponential growth of the solution and is easily detectable, instability in nonlinear problems is not always as easily detectable by mere viewing of the results. However, instability of nonlinear analyses can easily be detected by an energy balance check. Any instability leads to incorrect generation of energy which violates conservation of energy. Therefore, increase in the total energy of the analysis indicates instability in the analysis.

Abaqus (2017) presents the energy balance as

$$E_I + E_V + E_{FD} + E_{KE} + E_{IHE} - E_W - E_{PW} - E_{CW} - E_{MW} - E_{HF} = E_{total}, \tag{7}$$

where E_I is the internal energy, E_V is the viscous energy dissipated, E_{FD} is the frictional dissipated energy, E_{KE} is the kinetic energy, E_{IHE} is the internal heat energy, E_W is the work done by the external applied loads, E_{PW}, E_{CW} and E_{MW} are the work done by contact penalties, constraint penalties and propelling added mass and E_{HF} is the external energy through external fluxes. The sum of these energies is E_{total}. E_{total} should remain constant thorough the analysis. However, in numerical models this is seldom the case and E_{total} remains only approximately constant, generally within an error of less than 1%.

The internal energy E_I consists of several components. The expression for the internal energy is

$$E_I = E_E + E_P + E_{CD} + E_A + E_{DMD} + E_{DC} + E_{FC}, \tag{8}$$

where E_E is the recoverable elastic strain energy, E_P is the dissipated energy through inelastic processes such as plasticity, E_{CD} is the dissipated energy through viscoelasticity or creep, E_A is the artificial strain energy, E_{DMD} is the dissipated energy through damage, E_{DC} is the dissipated energy through distortion control and E_{FC} is the fluid cavity energy. (Abaqus 2017.)

Attention should be paid to the artificial strain energy E_A. It includes the energy stored in hourglass resistances and transverse shear in shell and beam elements. Large values of E_A indicate that mesh refinement or other changes to the mesh must be made.

2.4 Contact formulation

Many of the analyses of practical problems involve contact and impact. In crash simulation of automobiles many of the numerous components can come in contact during the crash and are treated as sliding interfaces. Treatment of impact always requires a treatment of contact as impacting bodies will stay in contact until rarefaction waves end up releasing them. (Belytschko et al. 2014, p. 597.)

2.4.1 Contact detection

Common way to detect contact in finite element analysis is the master-slave algorithm. The idea of master-slave algorithm is that two surfaces are specified, a master surface and a slave surface. Master surface is defined by the facets connecting the nodes of master surfaces elements. The slave surface is only defined as a set of nodes. Contact is detected when a node of the slave surface penetrates a facet of the master surface. Nodes of the master surface can penetrate the undefined facets of the slave surface without contact being detected. (Abaqus 2017.) This is illustrated in figure 1.

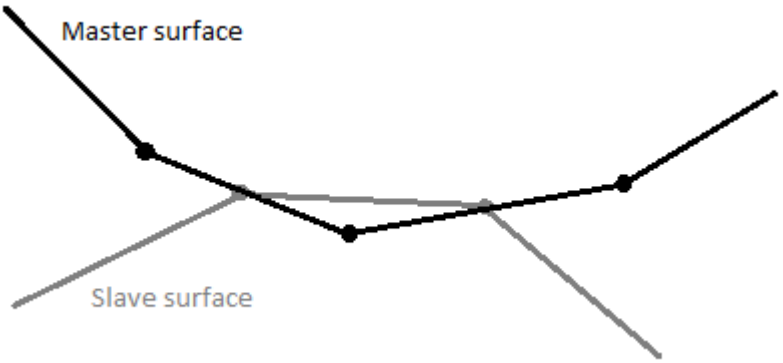

Figure 1. Master-slave node-to-surface contact.

2.4.2 Contact enforcement

Contact can be defined in Abaqus/Explicit with two methods, general contact and contact pairs. General contact automatically defines contact between every part that comes into contact with itself or other part. When using contact pairs, the user must determine the master and slave surface of the contacting parts. To enforce contact constraint Abaqus/Explicit uses two different methods: the kinematic contact algorithm and the penalty contact algorithm. The kinematic contact algorithm is automatically used with contact pairs and penalty contact algorithm with general contact.

Kinematic contact algorithm is a predictor/corrector algorithm. The kinematic state of the model is first advanced into predicted configuration. The predicted configuration is then checked for slave nodes that have penetrated the master surface. The penetration distance, mass associated with the penetrating nodes and the time increment are then used to calculate a resisting force required to stop the penetration. If the master surface is formed by element faces, the resisting forces are distributed to the nodes on master surface. The mass of the contacting slave nodes is also distributed to the nodes of the master surface so that the total inertial mass of the contact can be determined. These distributed forces and masses are then used to calculate the acceleration correction for the master surfaces nodes. Acceleration corrections for slave nodes are then determined using the predicted penetration distance, time increment and the acceleration corrections of the master surfaces nodes. These accelerations are used to obtain the corrected configuration in which contact is enforced. If the master surface is an analytical rigid surface, the resisting forces of all slave nodes are applied as generalized forces on the rigid surface. The mass of the contacting slave nodes is also added to the rigid surface to determine the total

inertial mass of the contact. The generalized forces and added masses are used to calculate the acceleration correction for the rigid master surface. Acceleration corrections for the slave nodes are determined from the corrected motion of the rigid master surface. Contact is enforced strictly by the kinematic contact algorithm and no penetration of slave nodes though master surfaces are allowed. However, when using pure master-slave detection algorithm, master nodes can still penetrate the slave surfaces.

Penalty contact algorithm searches for slave nodes that have penetrated the master surfaces faces in the current configuration. Forces that are a function of the penetration distance are applied to the slave nodes to oppose the penetration. Equal and opposite forces act on the master surfaces faces. The forces on master surface are distributed to the nodes of the master facets that have been penetrated. Similar to kinematic contact algorithm master nodes can penetrate slave surfaces. Penalty contact algorithm is less strict in enforcement of contact and some penetration can occur. It is however usable with more types of contact, rigid-to-rigid contact for example. Because the penalty contact algorithm introduces some stiffness behaviour into a model can it influence the stable time increment. Abaqus automatically accounts for the increased stiffness although the effect is most often small. (Abaqus 2017.)

3 OPTIMIZATION

Increase in global competition and demand for lower production costs is driving engineers to reduce the development time of new products. One way to achieve this is to discard the process where designer manually iterates to find a good-enough solution to a design problem typical of traditional product development and replace it with optimization. Recent advances in computer technology are enabling ever more complex and bigger problems to be solved.

3.1 Optimization formulation

Adams et al. (2018a, p. 123-124) give a general formulation for optimization problem as:

$$
\begin{aligned}
&\text{minimize:} && f(x) \\
& && \boldsymbol{x} \in \mathbb{R}^n \\
&\text{subject to:} && \boldsymbol{g}_L \leq \boldsymbol{g}(x) \leq \boldsymbol{g}_U \\
& && \boldsymbol{h}(x) = \boldsymbol{h}_t \\
& && \boldsymbol{a}_L \leq \boldsymbol{A}_i \boldsymbol{x} \leq \boldsymbol{a}_U \\
& && \boldsymbol{A}_e \boldsymbol{x} = \boldsymbol{a}_t \\
& && \boldsymbol{x}_L \leq \boldsymbol{x} \leq \boldsymbol{x}_U ,
\end{aligned}
\tag{9}
$$

where vector and matrix terms are marked in bold font. In this formulation, $\boldsymbol{x} = [x_1, x_2, \dots, x_n]$ is an n dimensional vector of real-valued design variables. The n-dimensional vectors, $\boldsymbol{x}_L$ and $\boldsymbol{x}_U$, are the lower and upper bounds of the design variables. The set of possible values defined by these bounds is called the design space. A particular combination of values within the design space is called a design point.

The goal of the optimization is to minimize the objective function $f(x)$ while satisfying the constraints. Constraints are categorized as either linear or nonlinear and as either inequality or equality. In formulation (9) $\boldsymbol{g}(x)$ is the nonlinear inequality constraint. It is 2-sided with upper and lower bounds $\boldsymbol{g}_U$ and $\boldsymbol{g}_L$. $\boldsymbol{h}(x)$ is the nonlinear equality constraint, which has target values specified by $\boldsymbol{h}_t$. Linear system $\boldsymbol{A}_i \boldsymbol{x}$ is created by the linear

inequality constraints. $\boldsymbol{A}_i$ is the coefficient matrix for the linear system. Linear inequality constraints are also 2-sided with upper and lower bounds $\boldsymbol{a}_U$ and $\boldsymbol{a}_L$. Linear system $\boldsymbol{A}_e\boldsymbol{x}$ is created by the linear equality constraints. $\boldsymbol{A}_e$ is the coefficient matrix for the linear system and $\boldsymbol{a}_t$ are the target values. Constraints divide the design space into feasible and infeasible "domains". A design point is feasible if it satisfies all constraints and infeasible if it violates one or more of the constraints.

3.2 Methods

The method selected to optimize a given problem is dictated by the characteristics of the problem. Not a single optimization algorithm is fit for all problem types (Shan & Wang 2010, p. 234). According to Adams et al. (2018a, p. 124) optimization problem types are described to be characterized by both the types of constraints applied to the problem and the linearity or nonlinearity of the objective function and constraint functions. Similar classifications are also given by Rao (2009, p. 14, 19) along with several other ways to classify optimization problems. Most applications of optimization to engineering problems are of the nonlinear type (Adams et al. 2018a, p. 124).

Additionally, the search goal significantly affects the selection of optimization method. Optimization methods locating global optimal points over the whole parameter space differ from methods locating local optimal points relatively near to the initial point. Generally, global optimization methods are computationally more expensive. When selecting the optimization method optimization goal and computational budget are the determining factors to be considered. (Adams et al. 2018a, p. 124.)

Optimization methods of nonlinear problems can be divided roughly into two categories. Adams et al. (2018a p. 126-129) names these categories "gradient-based" and "non-gradient-based". Rao (2009, p. 304) uses a different name for both categories although the categorization is essentially the same. He calls methods that do not require derivatives of the object function "Direct search methods" and methods that do require a derivative of the object function "Descent methods".

3.2.1 Gradient-based methods

Gradient-based methods are unsurprisingly based on gradient information. They can be of first or second order. First-order methods are based on the linear approximation of the

Taylor series and second-order methods are based on the quadratic approximation of the Taylor series. First-order methods entail the gradient and second-order methods entail the Hessian in addition of the gradient (Antoniou & Lu 2007, p. 119). Gradient-based methods experience some of the fastest convergence rates. However, gradients can be computationally expensive, inaccurate or not exist at all. If the problem is nonsmooth, discontinuous or exhibits multimodal behaviour gradient-based methods are not suitable. Gradient-based methods can only be used to find a local minimum. (Adams et al. 2018a, p. 126.)

3.2.2 Non-gradient-based local methods

Non-gradient-based methods or direct search methods use only the objective function evaluation to find the optimal solution. They are essentially an organized way to explore the design space. A simple non-gradient method would be to adjust all of the design variables of a starting point one by one and then select a new point based on the calculated values of the objective function. This would then be repeated for the new point and so forth (Antoniou & Lu 2007, p. 119). Non-gradient-based methods exhibit much slower convergence times than gradient based methods and thus are more computationally expensive. Despite this they often are desirable to use as they are much more robust than gradient-based methods and can be applied even when the objective function is discontinuous, nonsmooth or multimodal (Adams et al. 2018a, p. 127-128).

3.2.3 Non-gradient-based global methods

Description of non-gradient-based local methods applies to global methods. They also do not require gradient information and only use the objective function evaluation to locate the optimal solution. However, they require significantly more function evaluations than non-gradient-based local methods (Adams et al. 2018a, p. 128-129). Good example of modern non-gradient-based global optimization method, which is also available in Dakota, is genetic/evolutionary algorithm. Genetic algorithms mimic the principles of natural selection, breeding and mutation. An initial population of random design points is evaluated. Design variables are represented as strings of binary values that mimic chromosomes of natural genetics. Value of the object function evaluation corresponds to fitness in natural genetics. The best design points in terms of objective function value are allowed to survive, “reproduce” and evolve.

3.3 Selection of optimization method

Modern sophisticated computational models often do not have reliable derivative information available. Through modest amount of additional computing they might be extractable but this requires significant amount of invasive coding and precise knowledge of the simulation code. Moreover, access to the code is required and with commercial software, such as Abaqus, the source code is simply not available. In some situations, numerical derivatives can be computed but if the objective function or constraint function are even moderately noisy numerical derivatives are not useful. The results of the barrier crash test simulations are suspected to have more than modest amount of noise. Derivative-free methods are easy to implement which also makes them attractive (Koziel & Yang 2011, p. 61-63). For these reasons the optimization part of this thesis uses derivative-free optimization method.

We are going to use a local derivative-free method as the use of global derivative-free method is not feasible for the optimization part of this thesis. The computational cost of the model is significant and because the global methods require thousands of iterations the optimization would take an unreasonably long time to converge. Koziel and Yang (2011, p. 68) argue that in practice, often good local optima suffices. For the performance of the barrier assembly a good enough solution is sufficient.

Out of derivative-free optimization methods pattern search method is selected.

3.4 Pattern search

Pattern search methods navigate through the design space according to a stencil of defined search directions. The stencil is modified as the iteration proceeds. Although patterns search methods are local methods they have limited global search capabilities. If the initial stencil is large enough it is possible to step over local minima. (Adams et al. 2018a, p. 128.)

A common and the simplest family of pattern search methods are referred to as generalized pattern search. Generalized pattern search relies on local exploration of the design space. At any particular iteration a stencil is centered at the solution. The stencil (or a pattern) is the defined search directions of the design variables. The objective

function is then evaluated at a point in each search direction and if an improvement in the objective function is found the stencil is relocated to that point. The process is then repeated. If an improvement is not found the stencil size is reduced. The process is repeated until a stopping criterion is met. The stopping criterion can be, for example, the size of the stencil or the amount of change in the objective function. (Koziel & Yang 2011, p. 65.)

4 METHOD

The goal of this thesis is to develop a finite element model which can be used in combination with optimization process to find an optimal post profile for the roadside barrier. The steps taken in the process of finding the optimal post profile are described in this chapter. The process requires experimental crash test data. The test method and data obtained from the crash tests are both described in this chapter.

4.1 Process of simulation and optimization

The whole process from the development of the fem model to the review of the final dimensions of the post used in the roadside barrier is presented schematically in figure 2.

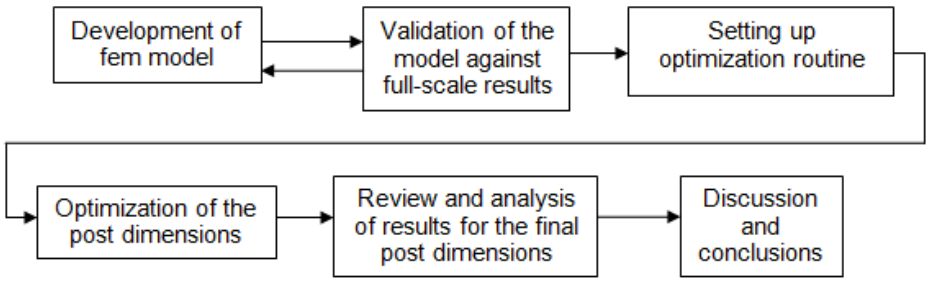

Figure 2. Schematic of the workflow for this thesis.

In order for a new post profile to be developed and optimized a finite element model of the car crashing to the barrier must be available. As stated previously Abaqus 2017 is used to develop the finite element model. In order for the model to be usable it has to be verified and validated. In a report of the National Academics of Sciences, Engineering and Medicine (2011, p. 9-13) called Procedures for Verification and Validation of Computer Simulations Used for Roadside Safety Applications verification and validation are described as follows: Verification is the process of determining that a computational model accurately represents the underlying mathematical model and its solution. Validation is the process of determining to which degree the model is an accurate representation of the real world from the perspective of the intended uses of the model. Model verification makes sure that the model obeys the basic physical laws. The total energy and momentum balance should not change beyond reasonable amount. Likewise, "non real" items, such as hourglass energy and added mass, should not grow beyond

agreed upon value. Table 1 is an analysis verification table provided in National Academics of Sciences, Engineering and Medicine (2011, p. E-3). The simulation should fulfil all the criteria listed in table 1 to be considered verified.

Table 1. Analysis verification table (retell National Academics of Sciences, Engineering and Medicine 2011, p. E-3).

Verification evaluation criteria	**Change (%)**	**Pass?**
Total energy of the analysis solution (i.e., kinetic, potential, contact, etc.) must not vary more than 10 percent from the beginning of the run to the end of the run.		
Hourglass Energy of the analysis solution at the end of the run is less than five percent of the total initial energy at the beginning of the run.		
Hourglass Energy of the analysis solution at the end of the run is less than ten percent of the total internal energy at the end of the run.		
The part/material with the highest amount of hourglass energy at the end of the run is less than ten percent of the total internal energy of the part/material at the end of the run.		
Mass added to the total model is less than five percent of the total model mass at the beginning of the run.		
The part/material with the most mass added had less than 10 percent of its initial mass added.		
The moving parts/materials in the model have less than five percent of mass added to the initial moving mass of the model.		
There are no shooting nodes in the solution?		
There are no solid elements with negative volumes?		

Validation involves any comparison between a numerical simulation and a physical experiment. SSAB has provided the results for several full-scale crash tests against which the model can be validated. The process of developing the fem model of the crash test was highly iterative and only the properties of final model are presented in this paper.

Once the fem model is determined to be reasonably accurate it can be paired with optimization software to determine the optimal post dimensions. Optimization software used is Dakota 6.8 developed by Sandia National Laboratories. It is an open source

software package free for download providing variety of methods for parameter study, optimization and uncertainty qualification among other things. Optimization methods include large variation of gradient-based, derivative free and global optimization methods. (Adams et al. 2018a, p. 21-23.)

Coupling Dakota to any simulation software is relatively simple. Adams et al. (2018a, p. 23-24) gives general explanation of the process. The interface consists of reading and writing simple data files. Dakota writes a parameter file which contains the design variables for the simulation. These parameters are then implemented into the simulation input file by any method chosen by the user. After the simulation has ran results are extracted from the simulation output file and written into a results file that can be read by Dakota. The process is then repeated with modified parameters. Dakota has no insight into the simulation software and only reads the result file and generates the parameter file. Because of this it is often referred as "black-box" coupling. Figure 3 presents a schematic of a general interface between Dakota and a simulation software or code. Dakota itself is executed with commands submitted by the user in an input file where the type of analysis is specified along with parameters, settings and file names of the user's simulation code. While operating Dakota automatically executes the user's simulation code.

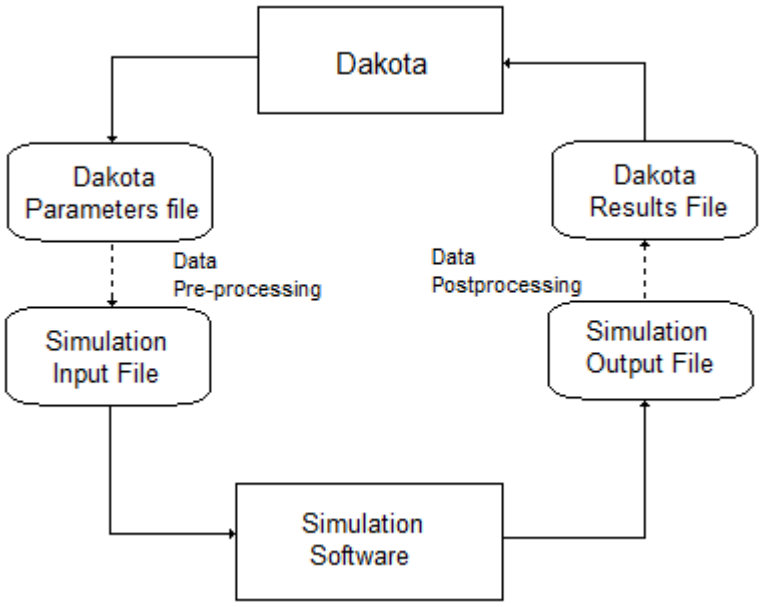

Figure 3. "Black-box" interface between Dakota and a simulation software/code (retell Adams et al. 2018a, p. 23).

4.2 Roadside barrier and crash test

To improve safety of roads installation of safety barriers alongside them is sometimes required. These barriers are intended to contain and redirect crashing vehicles. This containment and redirection benefits both the occupants of the crashing vehicle and other road users. The performance levels of the barriers, the requirements for the performance levels and the tests required to assess the performance level are given in the European Standard EN 1317-2. More detailed description of the crash test and its requirements are given is European Standard EN 1317-1. Additionally, calculation procedures and methods of recording crash impact data to assess impact severity levels are also given in European Standard EN 1317-1.

The crash test is set up so that the safety barrier to be tested is installed to conform to the way it would be installed on actual roads. A vehicle with determined mass is crashed to the installed barrier at a determined speed and angle. Types of tests with corresponding type of vehicle, vehicle mass, impact speed and impact angle are shown in table 2. The types of tests that are required for the barrier are determined by the containment level the barrier is designed for. A picture from the crash test reports provided by SSAB of the test setup for TB32 impact test just before the impact and 100 ms after it is shown in figure 4 to better illustrate the test.

Table 2. Impact test descriptions (retell EN 1317-2 2010, p. 7).

Test	Impact speed [km/h]	Impact angle [deg]	Total mass [kg]	Type of vehicle
TB11	100	20	900	Car
TB21	80	8	1300	Car
TB22	80	15	1300	Car
TB31	80	20	1500	Car
TB32	110	20	1500	Car
TB41	70	8	10000	Rigid HGV
TB42	70	15	10000	Rigid HGV
TB51	70	20	13000	BUS
TB61	80	20	16000	Rigid HGV
TB71	65	20	30000	Rigid HGV
TB81	65	20	38000	Articulated HGV

Figure 4. TB32 impact test just before the impact and 100 ms after the impact.

The performance of the barrier system is determined by three main criteria for which values are obtained from the crash test. The tree criteria are containment level, impact severity levels and the deformation of the barrier.

4.2.1 Containment levels

Containment levels and their requirements are described in EN 1317-2 (2010, p. 7-9). For the car to be contained it is required that the barrier stays intact during the crash and that the car does not pass over or under the barrier. The containment levels for safety barriers are presented in table 3. In table 3 are also presented the impact tests the barrier has to pass for each containment level. A general description of each impact test is given earlier in table 2.

Table 3. Containment levels (retell EN 1317-2 2010, p. 8).

Containment levels		Acceptance test
Low angle containment	T1	TB21
	T2	TB22
	T3	TB41 and TB21
Normal containment	N1	TB31
	N2	TB32 and TB11
Higher containment	H1	TB42 and TB11
	L1	TB42 and TB32 and TB11
	H2	TB51 and TB11
	L2	TB51 and TB32 and TB11
	H3	TB61 and TB11
	L3	TB61 and TB32 and TB11
Very high containment	H4a	TB71 and TB11
	H4b	TB81 and TB11
	L4a	TB71 and TB32 and TB11
	L4b	TB81 and TB32 and TB11

4.2.2 Impact severity

Impact severity levels are described in EN 1317-2 (2010, p. 9) and the methods to assess them are described in EN 1317-1 (2010, p. 17-24). The severity of the impact to occupants of the vehicle is assessed by recording the accelerations of the vehicle near its centre of mass and calculating two values from them, acceleration severity index (ASI) and theoretical head impact velocity (THIV). The levels of impact severity are presented in table 4.

Table 4. Impact severity levels (retell EN 1317-2 2010, p. 9).

Impact severity level	Index values	
	ASI	THIV
A	≤ 1.0	≤ 33 km/h
B	≤ 1.4	≤ 33 km/h
C	≤ 1.9	≤ 33 km/h

ASI is calculated from the three components A_x, A_y, A_z of recorded vehicle acceleration. The unit of measure is gravitational acceleration g. To calculate ASI the data must first be filtered with four-pole phaseless Butterworth filter with a 13 Hz cut-off frequency. ASI can then be calculated as a function of time as follows:

$$\mathrm{ASI}(t) = \sqrt{\bar{A}_x^2 + \bar{A}_y^2 + \bar{A}_z^2}\,, \tag{10}$$

where $\bar{A}_x$, $\bar{A}_y$ and $\bar{A}_z$ are the filtered components of vehicle acceleration. The ASI to describe the impact severity is the maximum of ASI(t).

Theoretical head impact velocity has been developed to assess the severity of the impact to the passenger in a collision with a roadside barrier or other kinds of road vehicle restraint systems. The passenger (or the head of the passenger) is considered to be a freely moving object that continues to move with the same speed and in the same direction as the vehicle pre-impact even after the vehicle itself changes its speed and direction due to the contact with the roadside barrier. The head eventually comes to contact with the interiors of the vehicle. The theoretical speed at which the head impacts the interiors of the car is used as a measure of the impact severity.

In the calculation of THIV two reference frames are used. A "vehicle" reference frame C_{xy} and a "moving ground" reference frame C_{XY}.

The vehicle reference frame moves with the vehicle and the origin C_{xy} is fixed to a point coincident or near the vehicles centre of mass. For the vehicle reference frame x is longitudinal (positive forwards) and y transverse (positive to the right). The reference frame is allowed to rotate around the z axis (yaw) but not around x and y axes (roll and pitch).

The moving ground reference frame C_{XY} is coincident with the vehicle axis C_{xy} at time t=0. It also has the same initial velocity as the vehicle. The moving ground frame is inertial and moves with constant velocity and does not rotate. As the freely moving head also moves at constant velocity before striking a surface its co-ordinates in the moving ground reference frame remain constant until the impact.

With the accelerations of the car A_x and A_y and yaw Ψ and rate of yaw $\dot{\Psi}$ recorded in the vehicle reference frame THIV can be calculated as follows:

First, the vehicle motion in the moving ground reference frame must be calculated. Vehicle accelerations $\ddot{X}_C$ and $\ddot{Y}_C$ in ground reference can be calculated with the recorded accelerations and yaw:

$$\begin{cases} \ddot{X}_C = A_x cos\Psi - A_y sin\Psi \\ \ddot{Y}_C = A_x sin\Psi - A_y cos\Psi \end{cases}, \tag{11}$$

Vehicle velocity $\dot{X}_C$ and $\dot{Y}_C$ and position X_C and Y_C in the ground reference can be integrated from the accelerations:

$$\begin{cases} \dot{X}_C = \int_0^t \ddot{X}_C \, dt \\ \dot{Y}_C = \int_0^t \ddot{Y}_C \, dt \end{cases}, \tag{12}$$

$$\begin{cases} X_C = \int_0^t \dot{X}_C \, dt \\ Y_C = \int_0^t \dot{Y}_C \, dt \end{cases}. \tag{13}$$

The initial conditions of the head in the moving ground reference frame depend on the heads position in the vehicle relative to the origin C_{XY}. Distances x_0 and y_0 are the initial distances x and y of the head from C_{XY} at t=0 (usually y_0 is taken as 0). The initial conditions at t=0 of the head in the moving ground reference frame are:

$$\begin{cases} X_b(0) = x_0; \; Y_b(0) = y_0 \\ \dot{X}_b(0) = 0; \; \dot{Y}_b(0) = 0 \end{cases}, \tag{14}$$

where subscript b denotes "head".

As previously stated, the head's co-ordinates and velocity remain constant in the moving ground reference frame until it impacts on a surface. Since the vehicle co-ordinates are

fixed to the vehicle, the displacement and velocity of the vehicle remain always zero in the vehicle co-ordinates. Thus, the displacement and velocity of the head relative to the vehicle is negative of the position and velocity of the vehicle relative to the moving ground reference frame:

$$\begin{aligned} X_b &= x_0 - X_C;\ \dot{X}_b = -\dot{X}_C \\ Y_b &= y_0 - Y_C;\ \dot{Y}_C = -\dot{Y}_C \end{aligned} \quad (15)$$

The displacement and velocity of the theoretical head compared to the vehicle reference frame can therefore be calculated from the displacements of the vehicle relative to the moving ground reference frame as follows:

$$\begin{aligned} x_b(t) &= (x_0 - X_C)cos\Psi + (y_0 - Y_C)sin\Psi \\ y_b(t) &= -(x_0 - X_C)sin\Psi + (y_0 - Y_C)cos\Psi \end{aligned} \quad (16)$$

$$\begin{aligned} \dot{x_b}(t) &= -\dot{X}_C cos\Psi - \dot{Y}_C sin\Psi + y_b(t)\dot{\Psi} \\ \dot{y_b}(t) &= \dot{X}_C sin\Psi - \dot{Y}_C cos\Psi - x_b(t)\dot{\Psi} \end{aligned} \quad (17)$$

The interior surfaces of the car the theoretical head impacts on are assumed to be flat and perpendicular to the vehicle reference frames x and y axes. The distances of the theoretical head from the surfaces at t=0 (flail distances) are D_x forward and D_y lateral. See figure 5 for an illustration of the theoretical head impacting on a surface on the left.

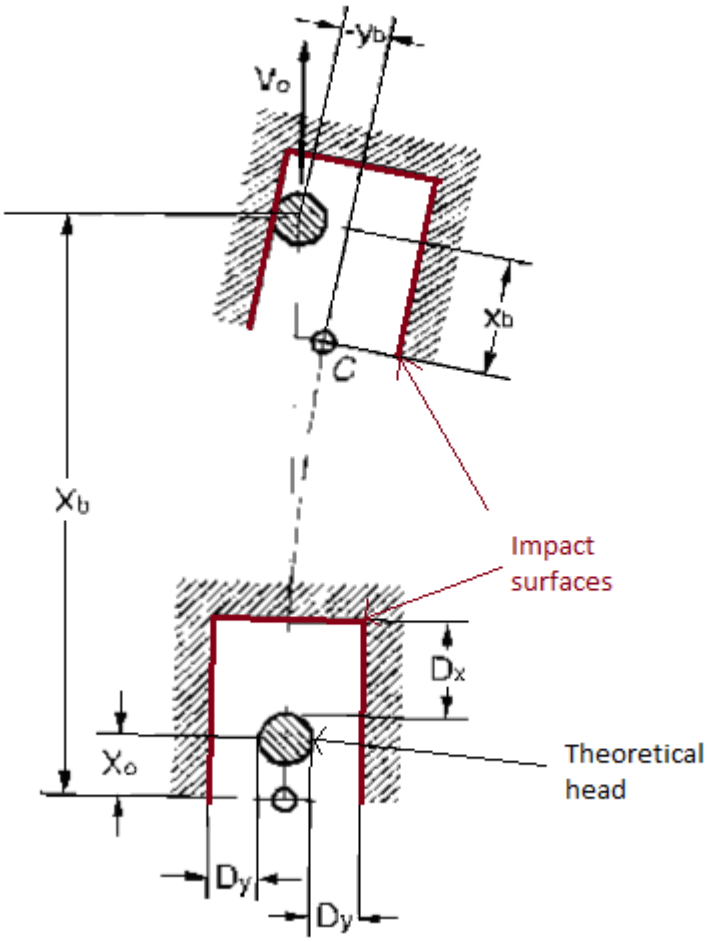

Figure 5. Theoretical head impacting on a surface on the left (retell EN 1317-1 2010, p. 22).

The time it takes for the head to impact on any of the impact surfaces is called time of flight. It is the shortest time T when any of the following three conditions are satisfied:

$$x_b(\mathrm{T}) = D_x + x_0; or\ y_b(\mathrm{T}) = D_y; or\ y_b(\mathrm{T}) = -D_y. \tag{18}$$

Standard distances the flail distances D_x and D_y are:

$$\begin{aligned} D_x &= 0.6\ m \\ D_y &= 0.3\ m \end{aligned} \tag{19}$$

With the time of flight T, the theoretical head impact velocity can be calculated as:

$$\mathrm{THIV} = \sqrt{\dot{x}_b^2(\mathrm{T}) + \dot{y}_b^2(\mathrm{T})}. \tag{20}$$

4.2.3 Deformation of the barrier

The deformation levels and methods to assess them are described in EN 1317-2 (2010, p. 9-13). The deformation characteristics of the barrier are described by three values: dynamic deflection, working width and vehicle intrusion. Vehicle intrusion concerns only heavy goods vehicles. Dynamic deflection (D_m) is the maximum lateral displacement of any point of the barrier system during the crash. Working width (W_m) is the maximum lateral distance between any part of the traffic side of the barrier system and maximum dynamic position of the barrier. See figure 6 for an illustration to explain dynamic deflection and working width.

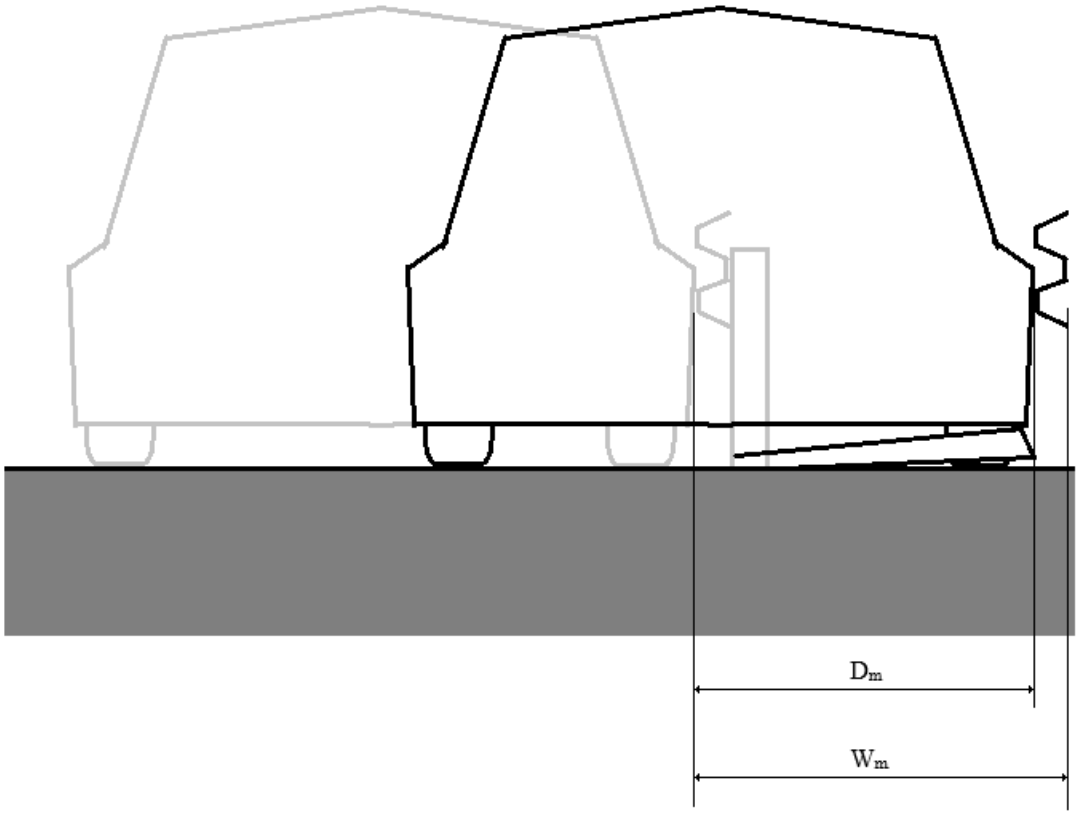

Figure 6. Illustration of dynamic deflection and working width (retell EN 1317-2 2010, p. 12).

Classes of normalised working width levels with the maximum allowed working width are shown in table 5.

Table 5. Levels of normalised working width (retell EN 1317-2 2010, p. 11).

Classes of normalised working width levels	Levels of normalised working width [m]
W1	$W_n \leq 0.6$
W2	$W_n \leq 0.8$
W3	$W_n \leq 1$
W4	$W_n \leq 1.3$
W5	$W_n \leq 1.7$
W6	$W_n \leq 2.1$
W7	$W_n \leq 2.5$
W8	$W_n \leq 3.5$

4.2.4 Additional requirements

Some restrictions and requirements for the behaviour of the vehicle apply during and after the impact and are listed in EN 1317-2 (2010, p. 15-16). The vehicle is not allowed to roll over. If it does the test is considered failed. Only one wheel of the vehicle is allowed to pass completely over or under the barrier during impact.

A major requirement is that the car has to leave the safety barrier after impact in such an angle that the wheel tracks don't cross a line parallel to the initial traffic face of the barrier system. The line is at distance of 2.2 m plus the width of the car plus 16% of the car length. The car shall not pass the line within a distance of 10 m from the last point P where the last wheel of the vehicle passes over the original line of the traffic side of the safety barriers face after the impact. The "exit box" is presented in figure 7 with a vehicle that passes the requirement and a vehicle that fails the requirement.

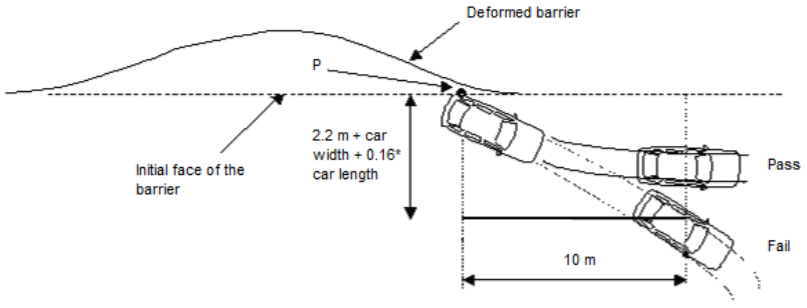

Figure 7. Exit box with example of a car that passes the requirement and a car which fails the requirement (retell EN1317-2 2010, p. 16).

5 SIMULATION MODEL

The model was developed for test types TB32 and TB11 as the barrier to be developed with optimization aims for containment class N2. SSAB provided test reports for several full-scale impact tests for both TB32 and TB11 types of tests. The simulation model was developed based on the information given in the test reports. In the reports were detailed descriptions of the barrier system tested, the crashing vehicle, deviations from the target speed and angle, material properties and results of performance. Table 6 presents all of the full-scale tests performed with the barrier length, post type, post spacing and impact speed defined.

Table 6. All test configurations of the performed full-scale tests.

Test	Rail length [m]	Post type	Spacing of posts [m]	Impact speed [km/h]
TB 32	96	Sigma	4	123
TB 11	96	Sigma	4	105
TB 32	96	U	4	114
TB 32	96	U	1	116
TB 11	96	U	4	101
TB 11	96	U	1	103
TB 32	72	U	4	110
TB 32	72	U	2	110
TB 11	72	U	4	106
TB 11	72	U	2	110

As stated previously and presented in figure 2, the development of the simulation model was highly iterative. The results obtained with the simulation model were constantly compared against the results from the full-scale tests. Many combinations of different setups and settings for the model were tried and only properties of the model setup that match best with the results of the full-scale tests are reported here.

5.1 Geometry

Results for five different barrier assemblies were provided by SSAB. The barrier assemblies differ by the geometry of the posts and rails, material used for post and rail, post spacing and the length of the assembly. TB 32 and TB 11 tests were run for all of the

different configurations of barrier assembly. In total 10 different configurations of the barrier assembly are required.

5.1.1 Barrier geometry

Two different kinds of posts are used in the barrier assemblies: Posts of type U and type sigma. Drawings for both types of posts are presented in figures 7 and 8.

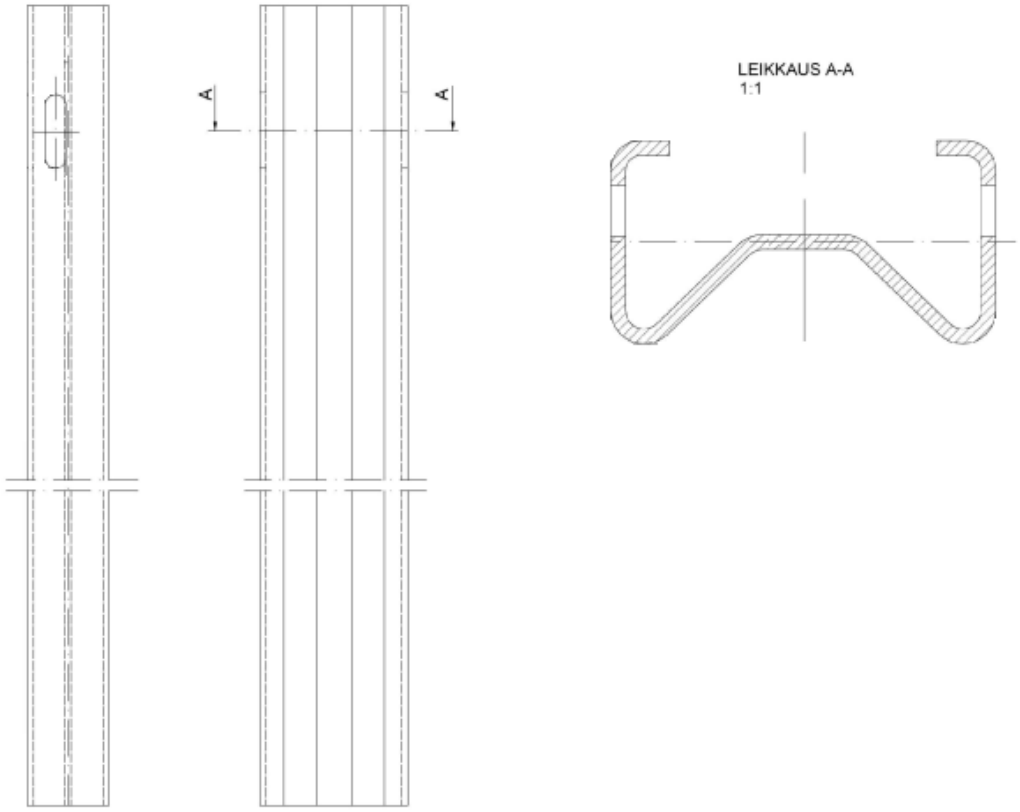

Figure 7. Drawing for post of type sigma.

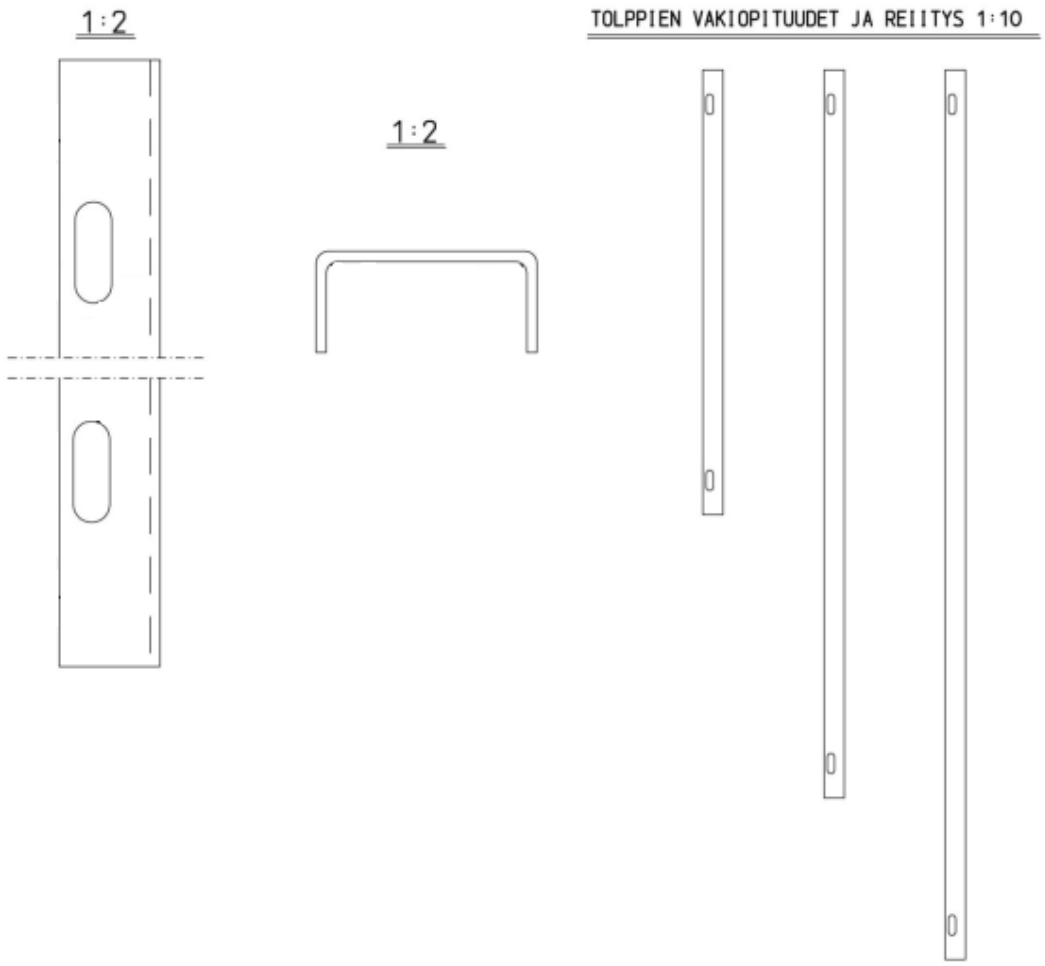

Figure 8. Drawing for post type U.

The long pieces that connect to the posts used in the barrier assembly are called rails. The rails are 12000 mm long and they are joined together by rail extension pieces. Two different kinds of rails and rail extension pieces are used in the barrier assemblies. However, they differ only in the thickness of the profile and material used. Rail used with sigma posts is 3 mm thick and manufactured out of steel grade S420MC. Rail used with U posts is 4 mm thick and manufactured out of steel grade S235. Drawings for the rail type used with sigma posts can be seen in figure 9 and for the type used with U posts in figure 10. Rail extension pieces are used to join the rails together. They appear every 12000 mm in the assembly. Similarly to the rails the extension pieces used with sigma and U posts differ only in the thickness and grade of the material used. The pieces used with sigma posts are 3 mm thick and made out of S420MC and the ones used with U posts are made 4 mm thick and made out of S235. Drawings for the rail extension pieces used with sigma posts are presented in figure 11 and for the pieces used with U posts in figure 12.

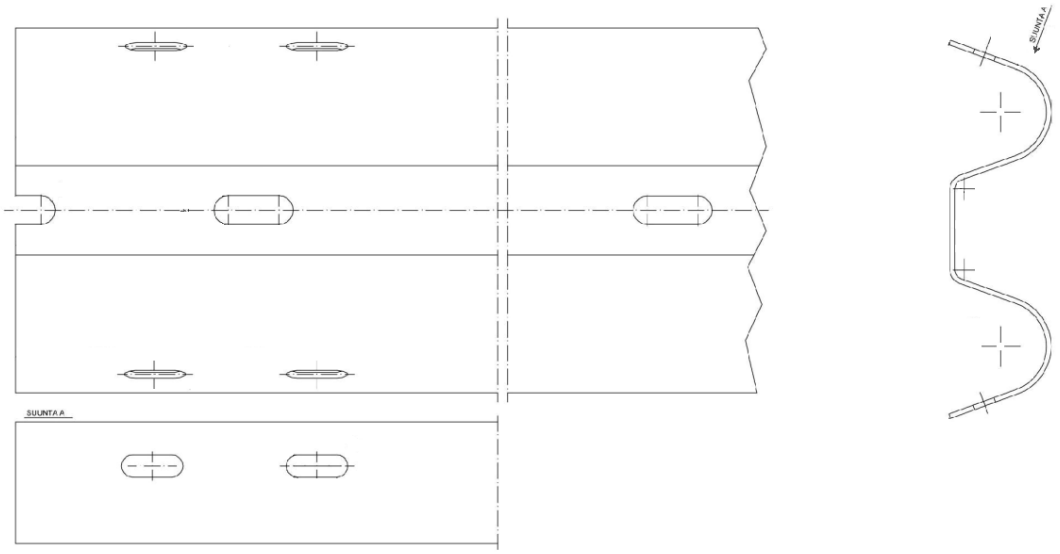

Figure 9. Drawing of the 3 mm thick rail used with sigma posts.

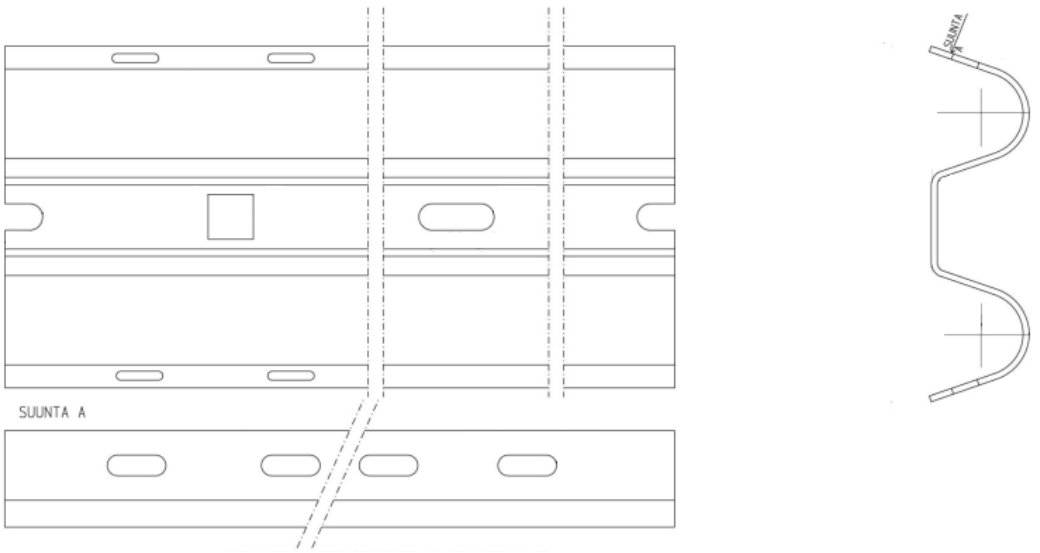

Figure 10. Drawing of the 4 mm thick rail used with U posts.

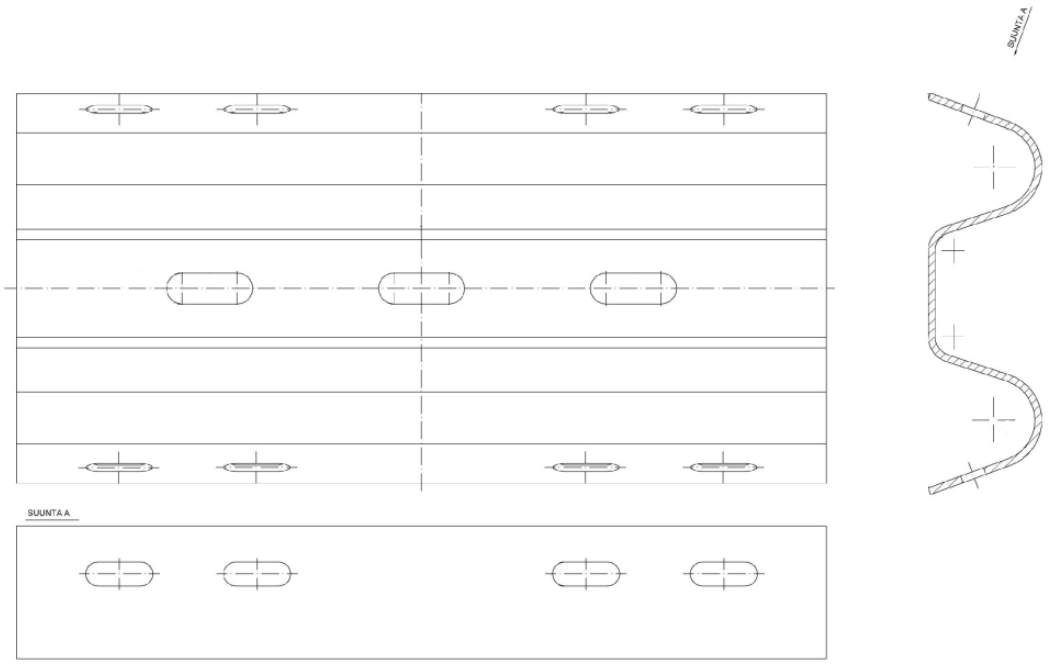

Figure 11. Drawing of the 3 mm thick rail extension piece.

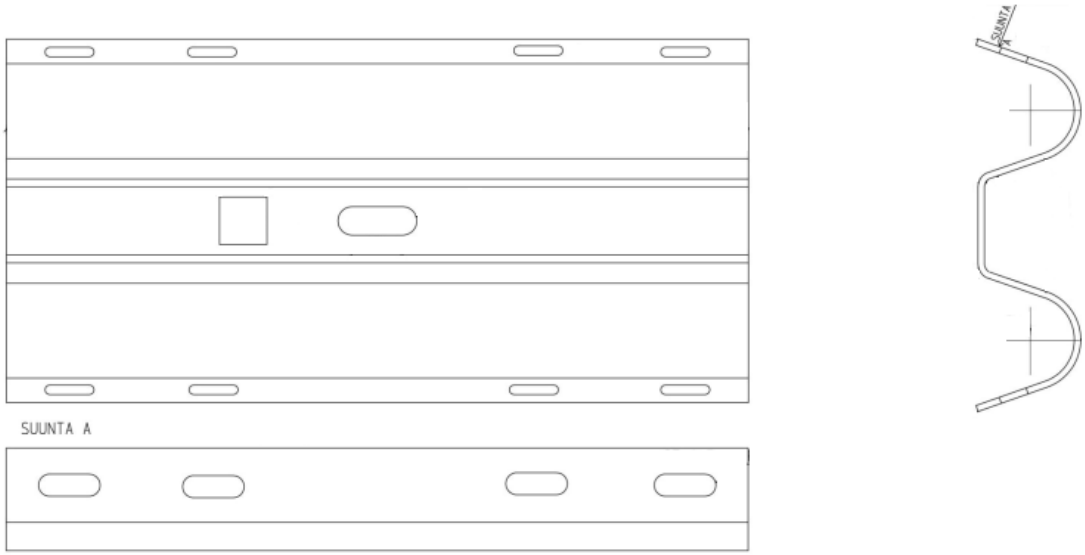

Figure 12. Drawing of the 4 mm thick rail extension piece.

The thin characteristics of the posts, rails and rail extension pieces make them suitable to be modelled as shells. The center line of the posts, rails and rail extension pieces profiles is extruded to create a 3D shell model. The surfaces of the shell models are then partitioned to provide geometrical points for connecting parts. Connections are discussed in chapter 5.4. Figure 13 shows the center line of sigma post to be extruded and the extruded 3D shell model. Figures 14-16 show the 3D shell model of the U post, rail and rail extension piece. Same shell model can be used for both types of rails and rail

extension pieces as they only differ in material and thickness and they are defined separately. Two pieces of rail for the beginning and end of the rail assemblies are modelled using the same profile as the regular rails. They differ slightly from the regular rails in that they have a small bend at one end so that they can rise and descend into the ground. Figure 17 shows a portion of the beginning/end piece with the bend. Fillets are removed from the modelled geometry as it would cause unnecessarily small elements to be present in the model. This would decrease the stable time increment and cause the run times for the simulations to increase.

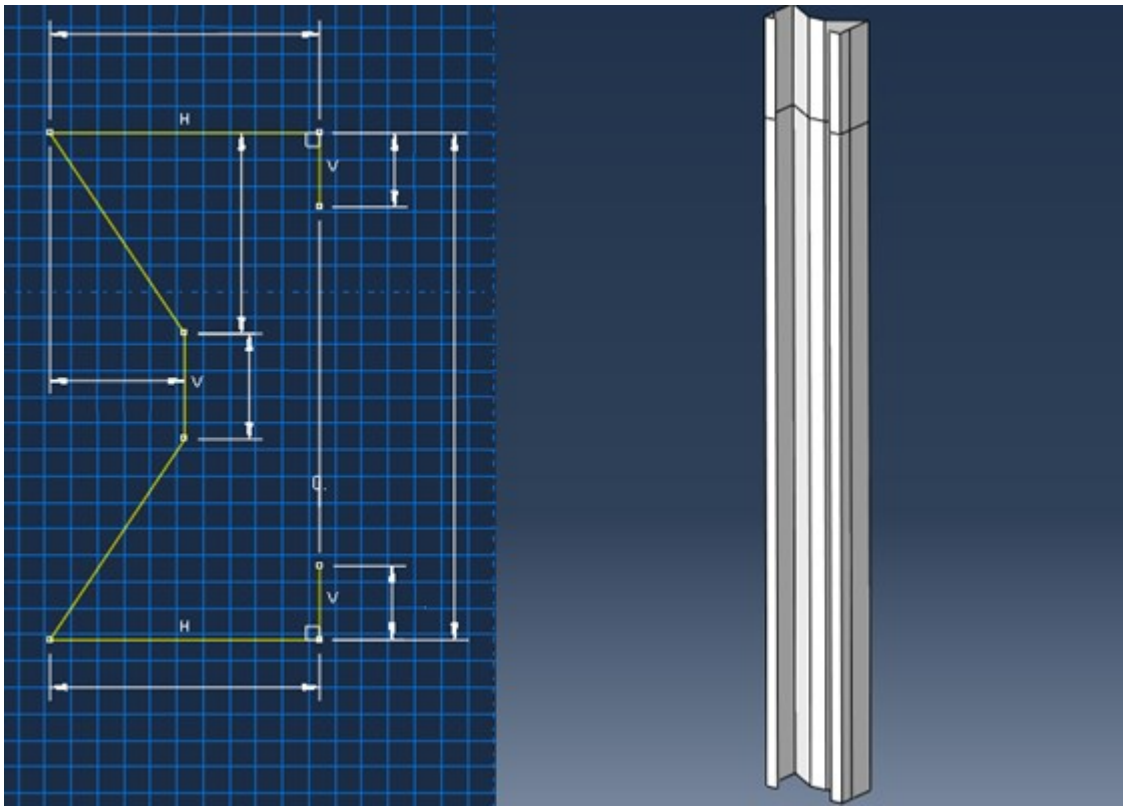

Figure 13. Center line of the sigma post profile to be extruded and the extruded 3D shell model.

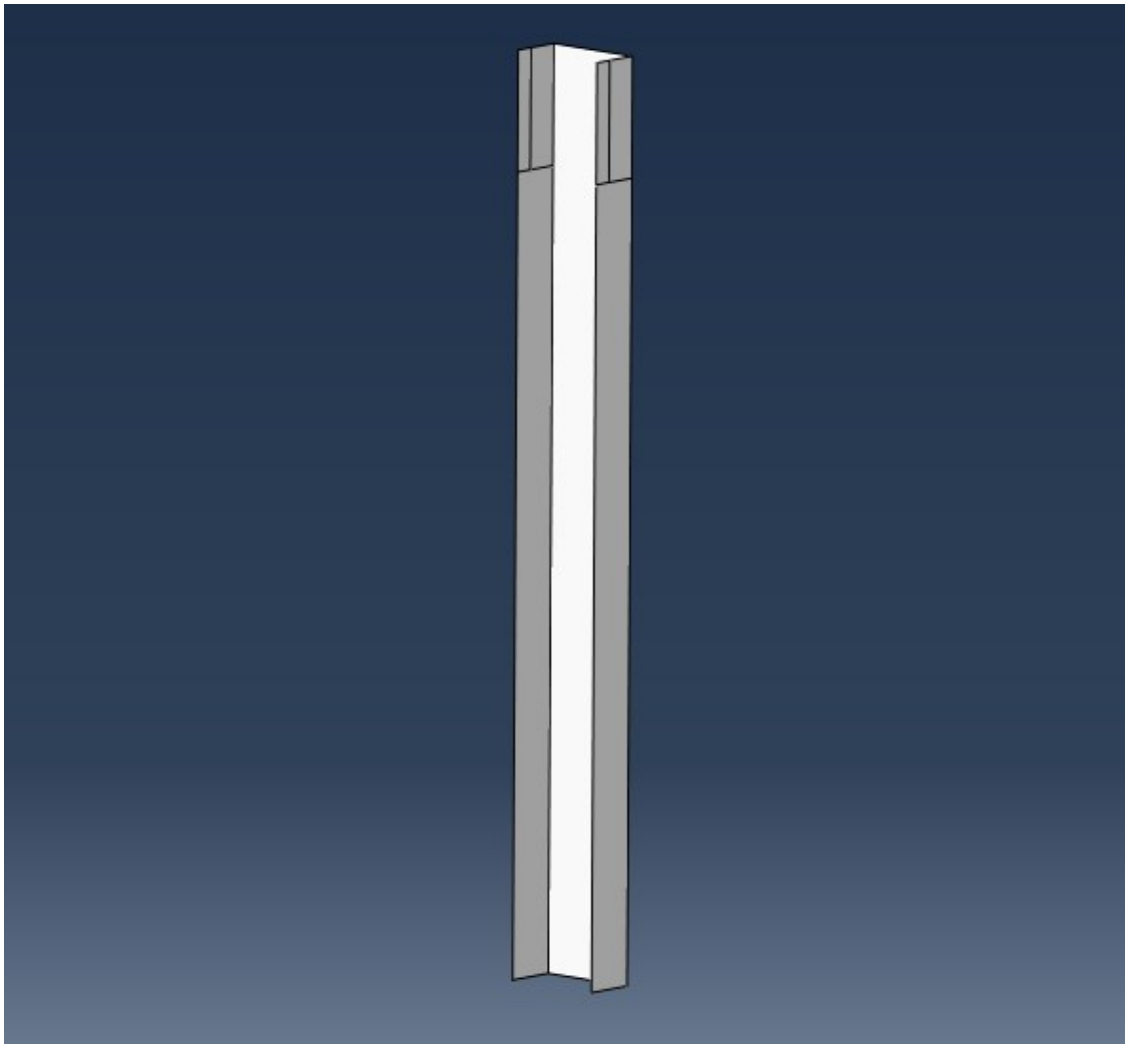

Figure 14. 3D shell model of the U post.

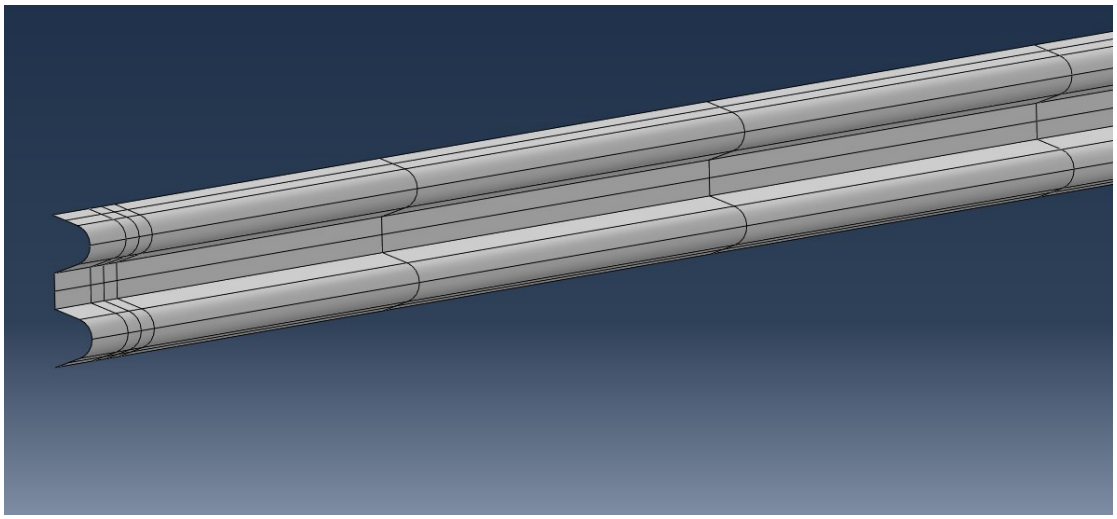

Figure 15. Partial view of the 3D shell model of the rail.

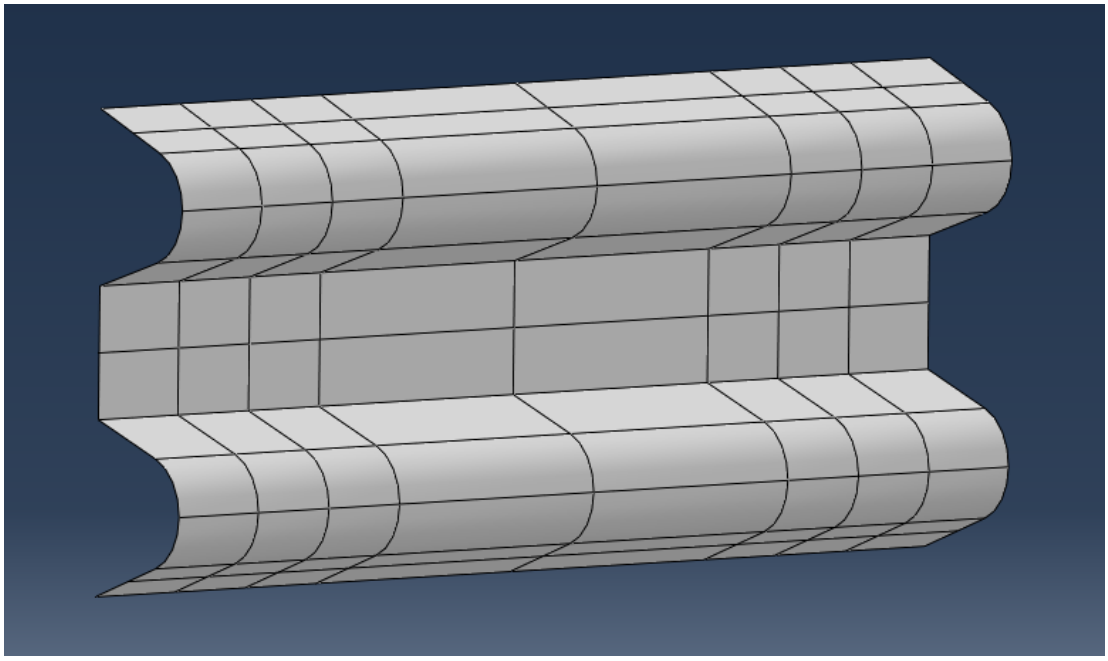

Figure 16. 3D shell model of the rail extension piece.

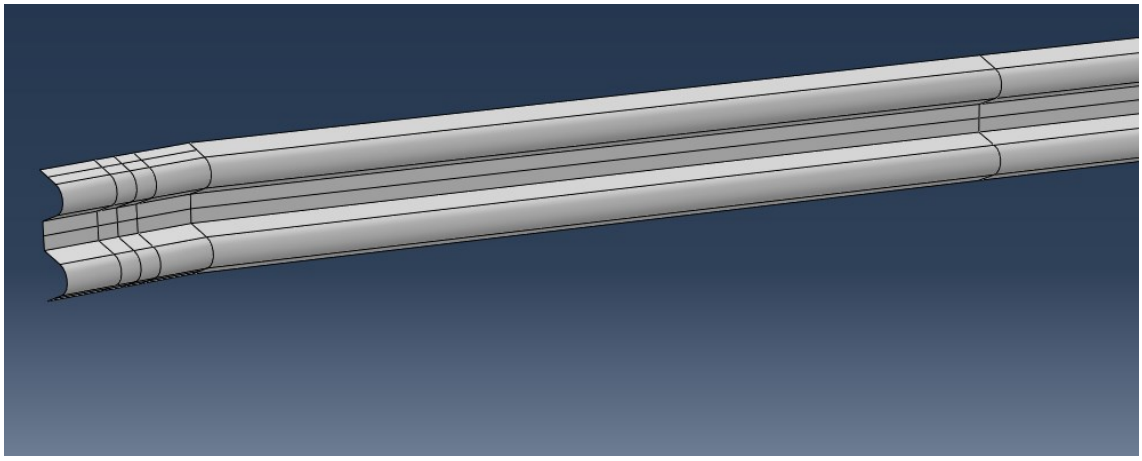

Figure 17. Beginning/end piece of the rail assembly with bend.

5.1.2 Car geometry

Cars used in the full-scale tests include Saab 9000, Peugeot 106, Talbot Horizon and Mercedes Benz 220 D. It would be a major effort and out of the scope of this thesis to develop a fem model for all of these cars. Accurate information of the cars might not even be easily available. In similar projects of simulating impact on roadside barrier models developed by National Crash analysis Centre (NCAC) have been used (Ren & Vesenjak 2005. p 967; Teng et al. 2016 p. 570). The models are based on Ford Taurus 2001 and Geo Metro. However, the models developed by NCAC are LS-DYNA models and they are not readily conversable to Abaqus. The models used in this thesis are developed after

the models of NCAC with matching dimensions and centre of mass. The masses of the cars are matched to the required weight for the test described in table 2.

The car models are modelled as shells. The mass and the location of centre of mass are matched to the models developed by NCAC by varying the thickness of the shells and density of the material of the shells. Less thick shells are used on the corners and sides of the cars to have them deform and absorb some of the impacts energy. Front and side views of the car model used in TB 32 tests can be seen in figure 18 and its dimensions and location of the centre of mass in table 7. Front and side views of the car model used in TB 11 tests can be seen in figure 19 and its dimensions and location of the centre of mass in table 8.

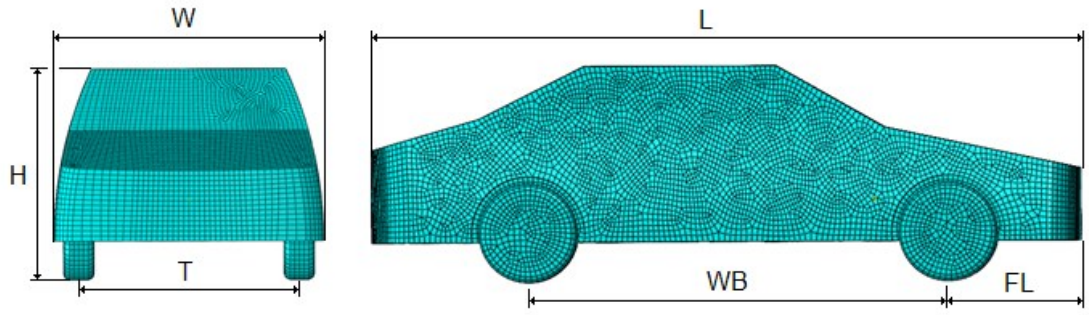

Figure 18. TB 32 car geometry from the front and side.

Table 7. TB 32 weight, dimensions and location of the centre of mass.

Vehicle dimensions and weight	
Weight	1500 kg
Length (L)	4.6 m
Width (W)	1.79 m
Height (H)	1.4 m
Wheel track (T)	1.58 m
Wheel radius	0.32 m
Wheel base (WB)	2.72 m
Front length (FL)	0.86 m
Centre of gravity location (from the front of vehicle)	
Longitudinal distance	1.15 m
Lateral distance	0 m
Height above ground	0.53 m

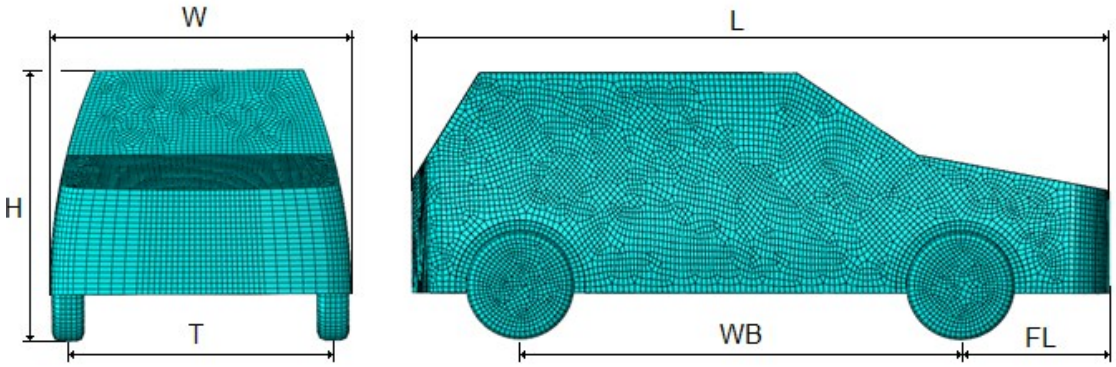

Figure 19. TB 11 car geometry from the front and sides.

Table 8. TB 11 weight, dimensions and location of the centre of mass.

Vehicle dimensions and weight	
Weight	900 kg
Length (L)	3.75 m
Width (W)	1.59 m
Height (H)	1.43 m
Wheel track (T)	1.4 m
Wheel radius	0.31 m
Wheel base (WB)	2.37 m
Front length (FL)	0.80 m
Centre of gravity location (from the front of vehicle)	
Longitudinal distance	0.8 m
Lateral distance	0 m
Height above ground	0.53 m

5.1.3 Assembly

Models were assembled according to the drawings in the full-scale test results. The top of the rail sits about 700 mm above the ground. The barriers are assembled as either 72 m or 96 m long. A rail extension piece is placed between every rail. The first piece of rail rises from the ground and the last piece descends into the ground over 12000 mm. The posts installed to the first and last portion of the rail are made shorter so that the bottom parts of the posts remain on the same level. Drawing for the installation of the first and last rail is shown in figure 20. The posts are placed so that the open portion of their profiles faces into the direction the car is moving. Exceptions are the first two posts of the assemblies which are installed with the open portion facing the opposite direction. Cars are placed in the models at a small distance away from the point of impact. There is no need for them to be placed further and travel longer distance before impact as the initial speed can be applied instantaneously. The impact point of all the models is 33.5 m from the first post. Figure 21 show TB 32 model with sigma posts. From the figure the direction the posts are installed can be seen.

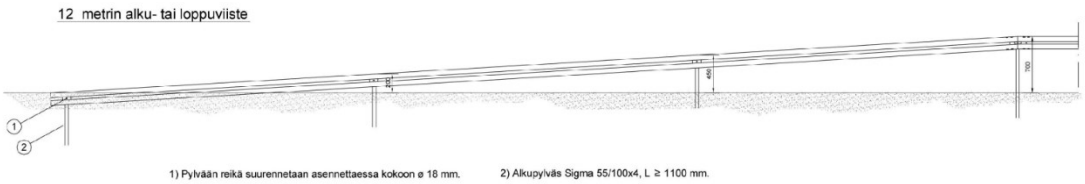

Figure 20. The descension/ascension of the first/last barrier.

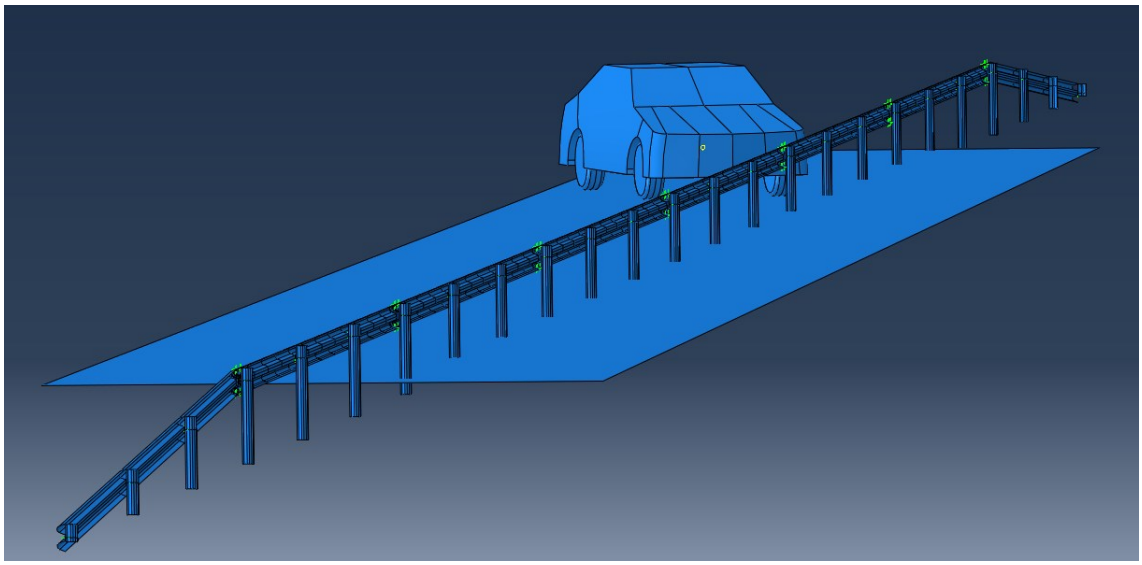

Figure 21. TB 32 model with sigma posts and 4 m post spacing.

Models differ also in the spacing of the posts. Crash tests were done with the posts installed at intervals of 4, 2 and 1 meters. In the assemblies with 1 m post spacing the spacing on the beginning and end rails differs from the regular rails. At the beginning and end rails the posts are placed at 2 m intervals. Figure 22 shows a rail assembly with U posts at 4 m intervals on the top and a rail assembly with U posts at 1 m intervals on the bottom.

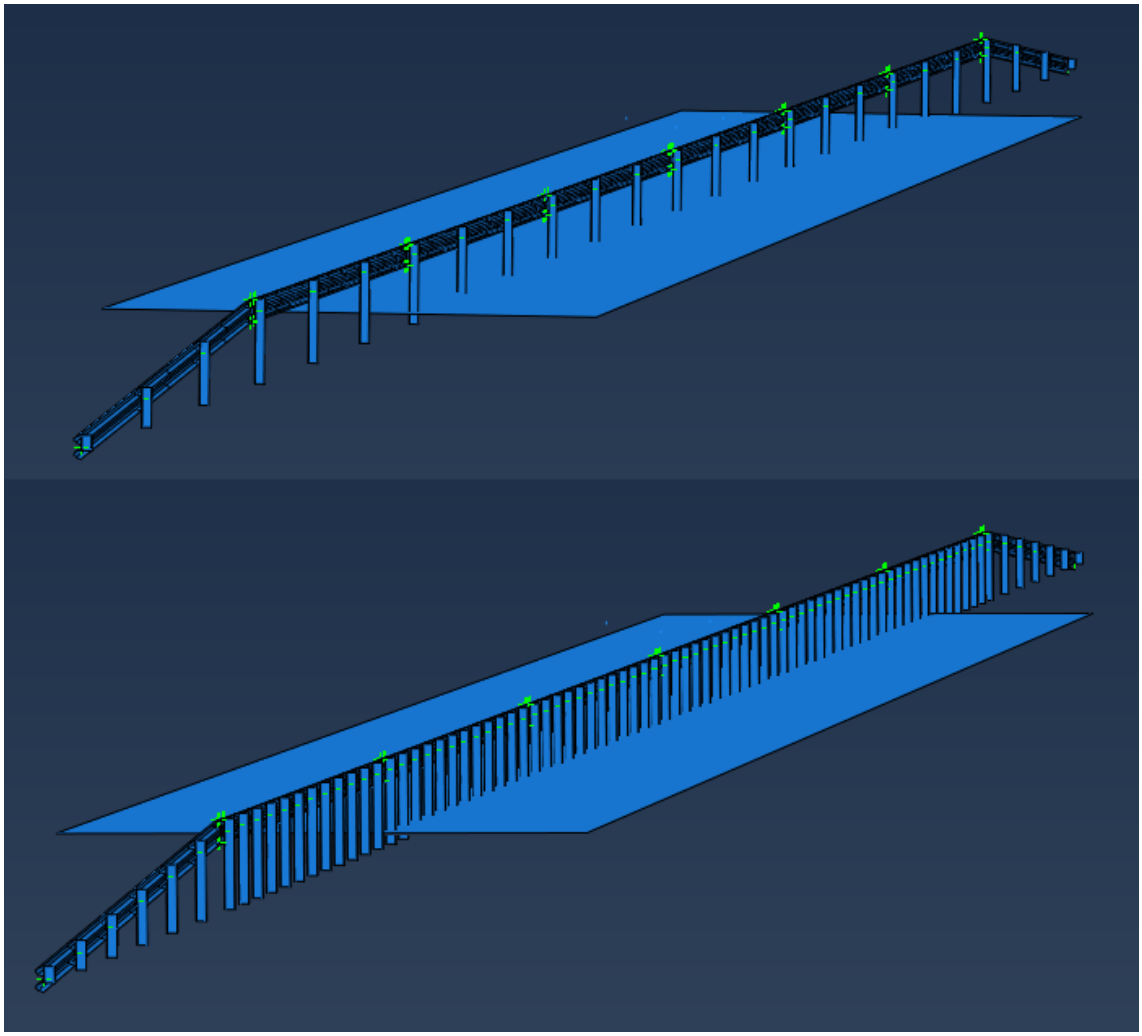

Figure 22. Rail assembly with U posts at 4 m intervals and rail assembly with U posts at 1 m intervals.

5.2 Material models

Material models used are elasto-plastic. As mentioned above, the U posts and the rail used with U posts are manufactured out of steel S235J2. The sigma posts are manufactured out of steel S355MC and the rail used with sigma posts out of steel S420MC. S355MC was used for both car models. SSAB provided tension test results for S355MC and S420MC to be used in the material model. Material data for S235J2 was derived from the test reports of the full-scale tests. It was provided for the test reports by the manufacturer. Youngs modulus used for all of the steels is 200 GPa, poisson ratio 0.3 and density 7850 kg/m^3.

5.3 Contact

A crucial part of an impact simulation is the implementation of contact. Abaqus has a general contact feature to automatically detect contacting parts. General contact was implemented to the whole model with a friction coefficient of 0.1. The contact between the tires of the cars and road was defined separately as surface-to-surface contact to allow for a different coefficient of friction. The coefficient was set to 0.5. The values for coefficient of friction were mainly decided upon comparing visually the trajectory of the car in simulations and full-scale tests. Contact between the posts and road was excluded because posts are fixed to have part of them below the road surface. Also, the models of the cars have no suspension implemented and having the posts get squeezed between the road and the tires would cause the car to bounce unrealistically. No contact between the road and posts gives more consistent results which is important for the optimization part of the thesis.

5.4 Connections

Various parts of the model have to be attached to other parts with connections.

The bolts connecting the rails to the posts are designed to break relatively easily and let the rail detach from the posts. Tension test results for the bolts were included in the full-scale test reports. To the model the bolts are implemented as mesh independent fasteners. The failure was implemented with the connector elements disappearing when any component of the forces acting in them reaches the ultimate strength of the bolts derived from the tension test results. This implementation correlated with the full-scale results. The bolts of the first two and last two posts were implemented as rigid as the bolts used in them are stronger. Implementing failure in these bolts is not required for accurate presentation of the impact event.

Rails were connected to the rail extension pieces with mesh independent fasteners. Figure 23 shows the locations of the connectors. The connectors are allowed to have some translational movement. A single connector is able to translate in plane linearly up to 10 mm as the force in the fastener increases to 10 kN. This was done to mimic the behaviour of the barrier in the crash tests. The joints were opening up in the crash tests. Figure 24

shows the opening of the joint from full-scale crash test after an impact and comparison to the opening of the joint from simulation.

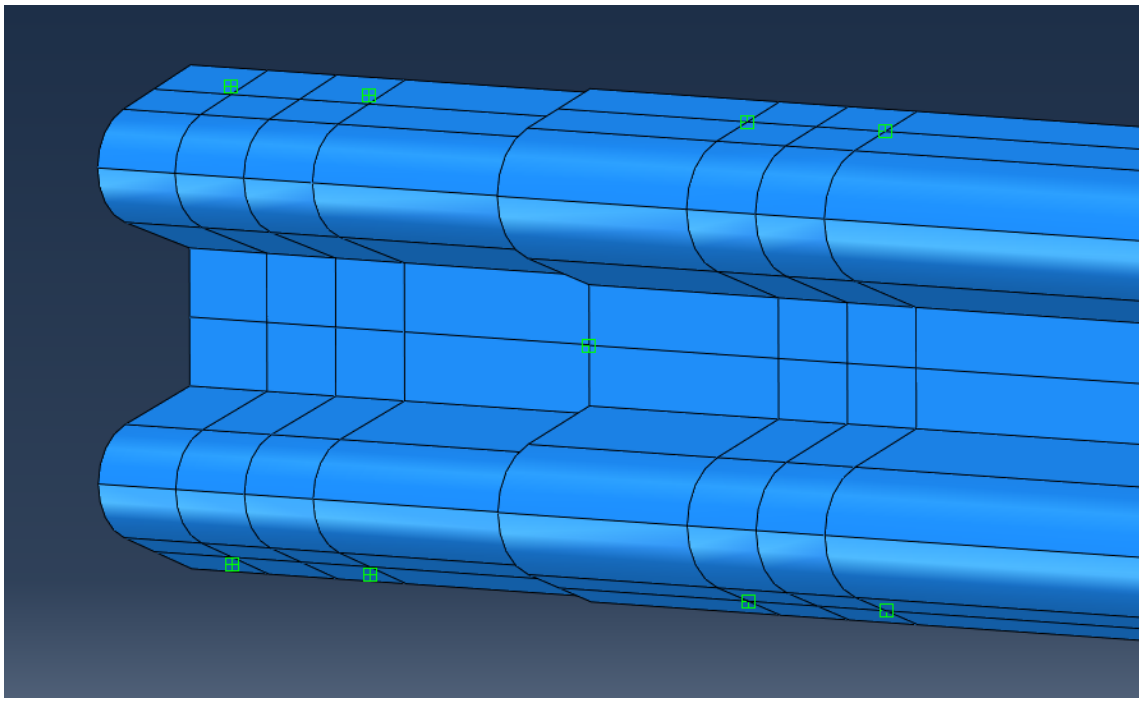

Figure 23. Locations of the connectors in the rails and rail extension pieces marked with green squares.

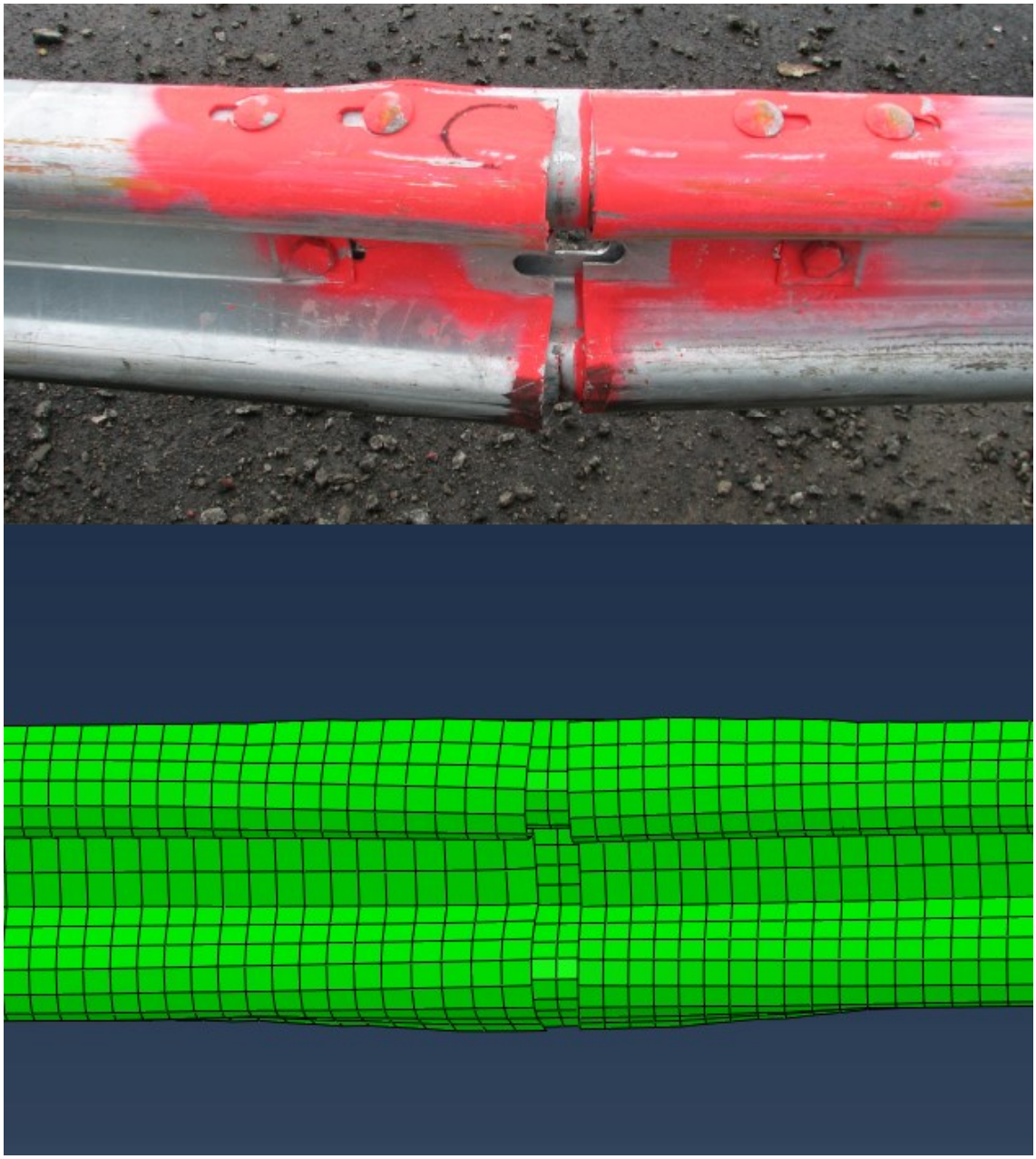

Figure 24. Comparison of the opening of the rails in full-scale tests and simulation.

To attach the tires of the cars to the body a kinematic coupling was implemented between the car side of the tires and a point on the axle of the tires and on a surface on the car and second point on the axle of the tires. The points the couplings are attached to are then joined with a hinge connector that allows the tires to rotate. The couplings and the hinge connector are presented in figure 25.

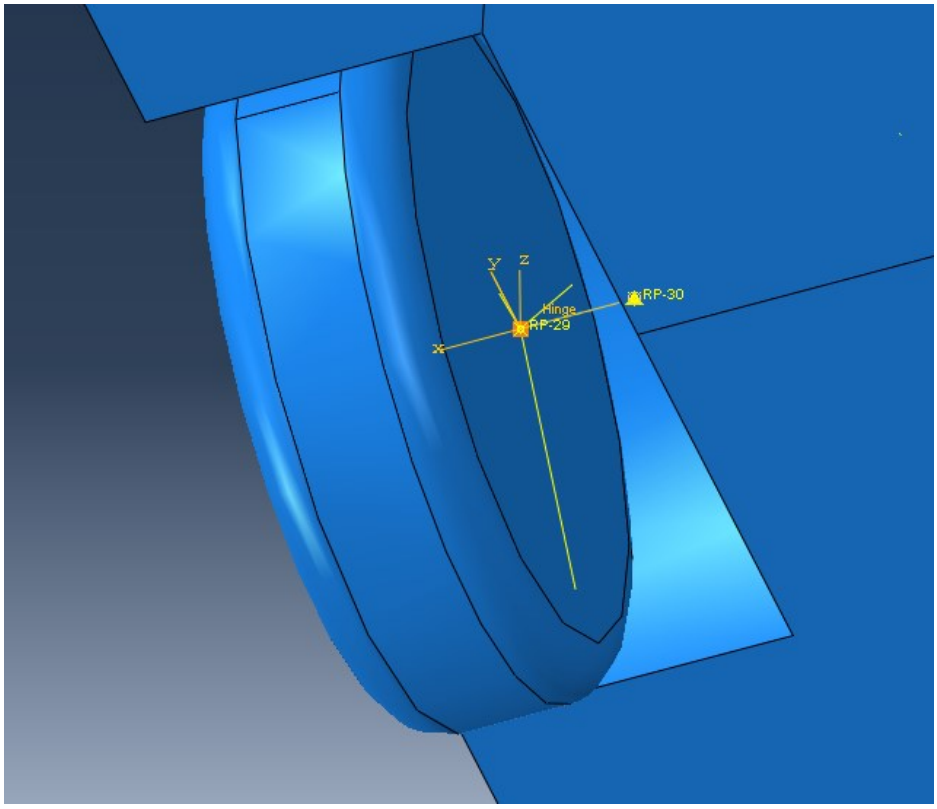

Figure 25. Coupling on the front right tyre of the TB 11 car and the hinge connector.

Some surfaces on the top and bottom of the cars are joined with a rigid coupling to the center of mass of the cars. This is done to provide rigidity to the cars and allow the recording of the accelerations from the centre of mass. Connected surfaces for both cars are presented in figure 26.

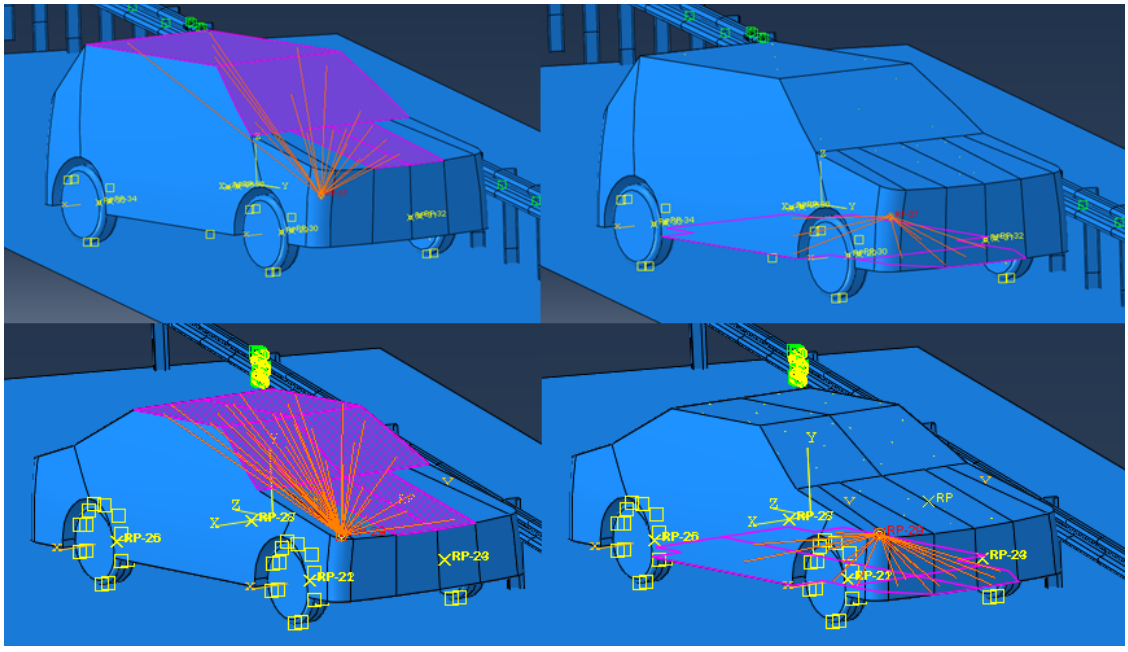

Figure 26. Surfaces connected to the center of mass for both cars.

5.5 Loads and constraints

5.5.1 Loads

A gravitational acceleration of 9810 mm/s^2 is applied to the whole model.

The velocity of the impacting cars is applied as a predefined field to the body of the cars. Tires are given a matching combined velocity and rotational velocity. Speeds for each test are given in table 6.

5.5.2 Constraints

The posts are constrained rigidly 150 mm below the ground. This is done to take the effect of the posts being installed into soil in account. Constraining the posts 150 mm below the ground gave good correlation with the full-scale tests.

5.6 Mesh

The barrier was meshed with 20 mm S4RS elements and the cars with 35 mm S4RS elements. S4RS is a 4-node shell element with reduced integration and small membrane strains. It is recommended for crash analysis by Crashworthiness analysis with Abaqus training material (2009 p. 146). The rigid road was meshed with 1000 m R3D4 4-node discrete rigid elements. The meshes of the cars can be seen in figures 17 and 18. The mesh of the barriers and posts can be seen in figure 27.

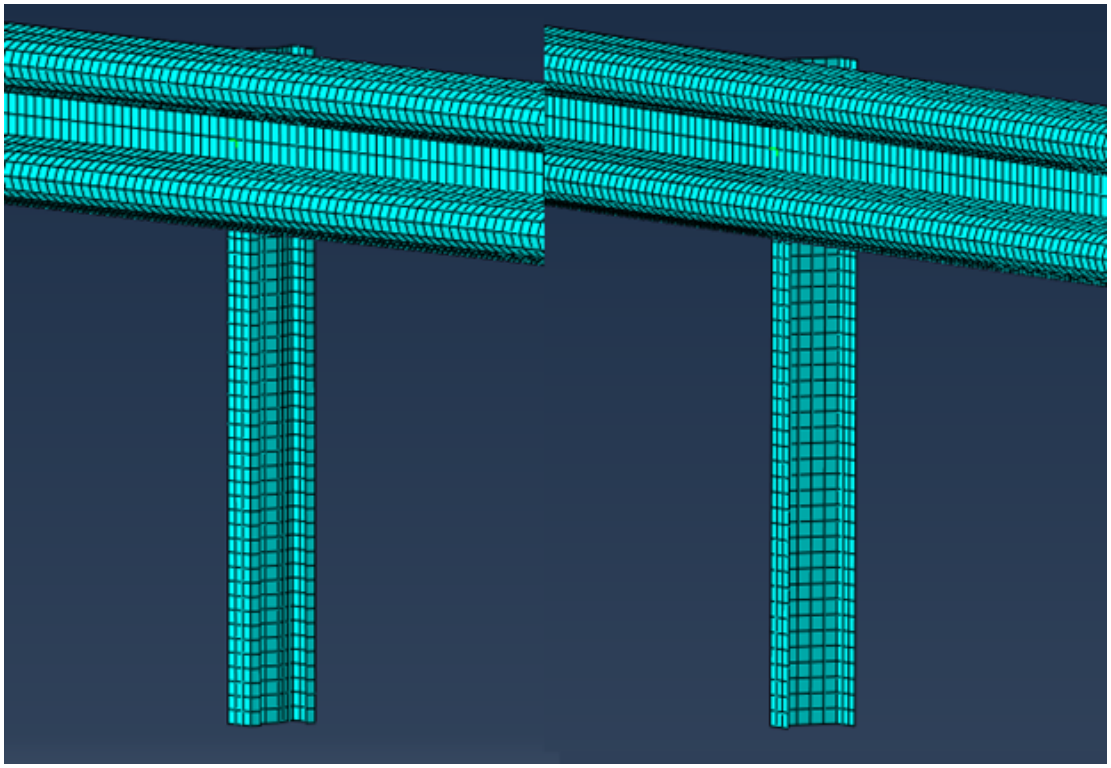

Figure 27. Mesh of the barrier with sigma and U posts.

5.7 Comparison of results

5.7.1 Verification

Model is considered verified as it passes all the requirements presented in analysis verification table. Filled analysis verification table for TB 32 simulation with sigma posts at 4 m intervals is presented in table 9. The verification results for this simulation can be considered as representative of all the simulations as the results were very similar. Total energy, internal energy, kinetic energy and artificial strain energy for the same simulation is presented in figure 28.

Table 9. Analysis verification table for TB 32 simulation with sigma posts at 4 m intervals.

Verification evaluation criteria	**Change (%)**	**Pass?**
Total energy of the analysis solution (i.e., kinetic, potential, contact, etc.) must not vary more than 10 percent from the beginning of the run to the end of the run.	-0.01	Yes
Hourglass Energy of the analysis solution at the end of the run is less than five percent of the total initial energy at the beginning of the run.	1.5	Yes
Hourglass Energy of the analysis solution at the end of the run is less than ten percent of the total internal energy at the end of the run.	5.2	Yes
The part/material with the highest amount of hourglass energy at the end of the run is less than ten percent of the total internal energy of the part/material at the end of the run.	-	Yes
Mass added to the total model is less than five percent of the total model mass at the beginning of the run.	0.04	Yes
The part/material with the most mass added had less than 10 percent of its initial mass added.	0.07	Yes
The moving parts/materials in the model have less than five percent of mass added to the initial moving mass of the model.	0.07	Yes
There are no shooting nodes in the solution?	No	Yes
There are no solid elements with negative volumes?	No	Yes

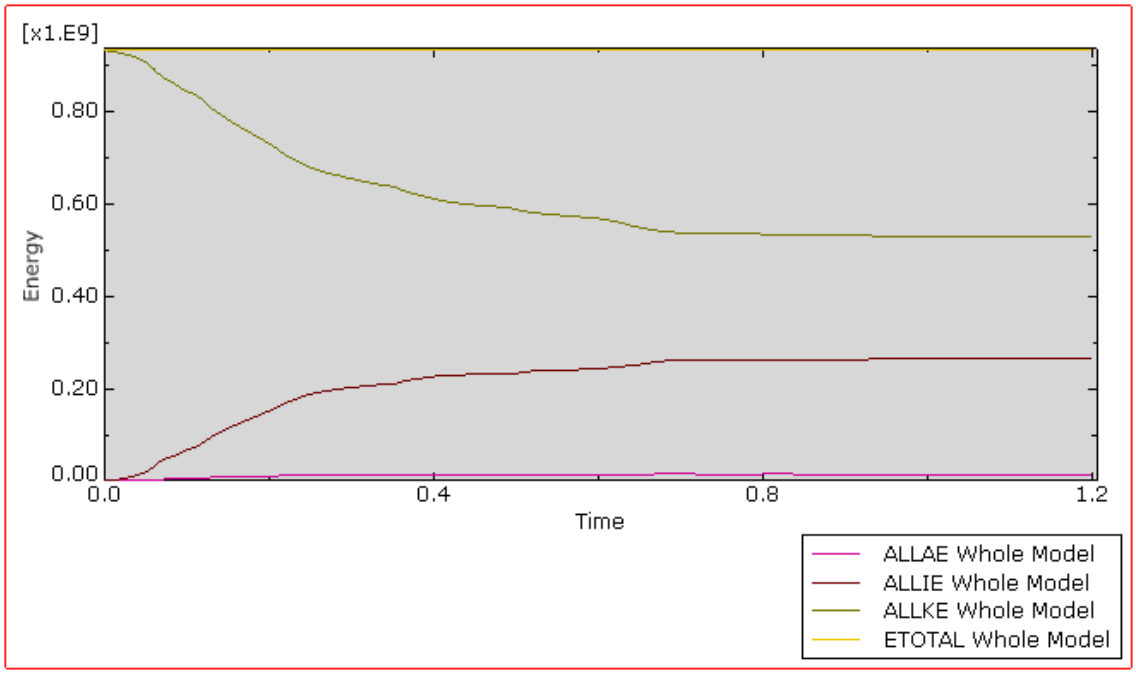

Figure 28. Total energy ETOTAL, Artificial strain energy ALLAE, Internal energy ALLIE and Kinetic energy ALLKE of TB 32 simulation with sigma posts at 4 m intervals.

5.7.2 Validation

A comparison between the full-scale test results and the results from simulation in terms of the percentual difference of measured dynamic deflection, ASI and THIV can be seen in table 10.

Table 10. A comparison between the full-scale results and simulations done with Abaqus.

				Difference %			
Rail Length	Test	Post type	Spacing	Impact speed [km/h]	Dynamic deflection	ASI	THIV
96	TB32	Sigma	4	123	-1.7	6	34
96	TB11	Sigma	4	105	-11.2	15	28
96	TB32	U	4	114	-10	14	24
96	TB32	U	1	116	10.5	7	22
96	TB11	U	4	101	-2.6	58	8
96	TB11	U	1	103	1.2	16	8
72	TB32	U	4	110	-12.5	-19	39
72	TB32	U	2	110	-16	50	19
72	TB11	U	4	106	-7.6	-1	27
72	TB11	U	2	110	-9.2	107	36

The target accuracy for all of the parameters was ±10%. The model falls short of this goal. However, for the models with 96 m long barrier dynamic deflection is barely out of the

target accuracy and ASI and THIV are significantly on the conservative side. Keeping the inaccuracy in mind and accounting for the higher ASI and THIV the model can be used to evaluate the performance of new barrier assemblies.

A comparison of ASI recorded from the full-scale test and the simulation of TB 11 test with sigma posts can be seen in figure 29 with the ASI of the simulation on top and ASI recorded during a full-scale test on the bottom. Even though the simulation experiences higher ASI the shape of the graph during the impact at 0 – 0.5 s is very similar.

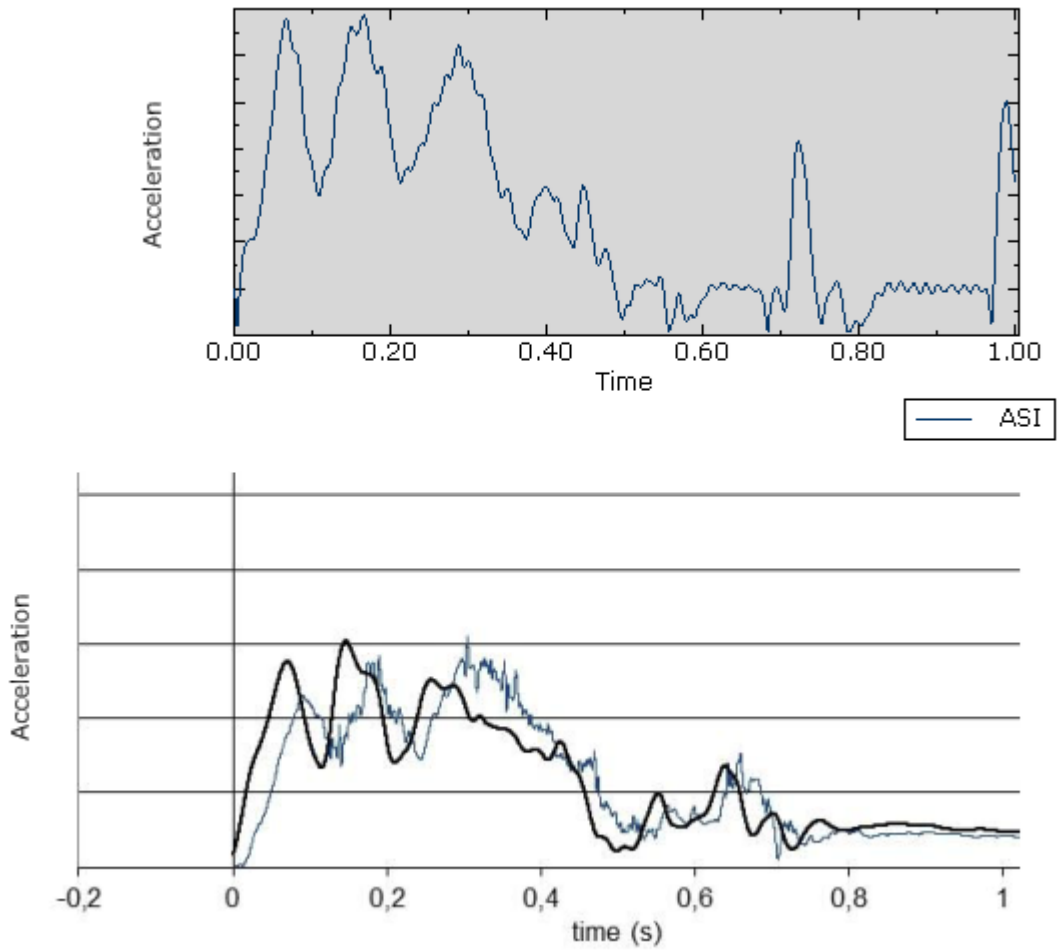

Figure 29. Comparison between ASI recorded from the full-scale test and simulation of TB 11 test with sigma posts at 4 m intervals.

To compare the trajectories of the cars in full-scale tests and simulations we can look at periodically taken photos of the impact events. Figure 30 shows a comparison of the impact event between the full-scale test and simulation of TB 32 test with sigma posts. Even though the car exits the barrier earlier in simulation the trajectories of the cars are very similar by visual comparison.

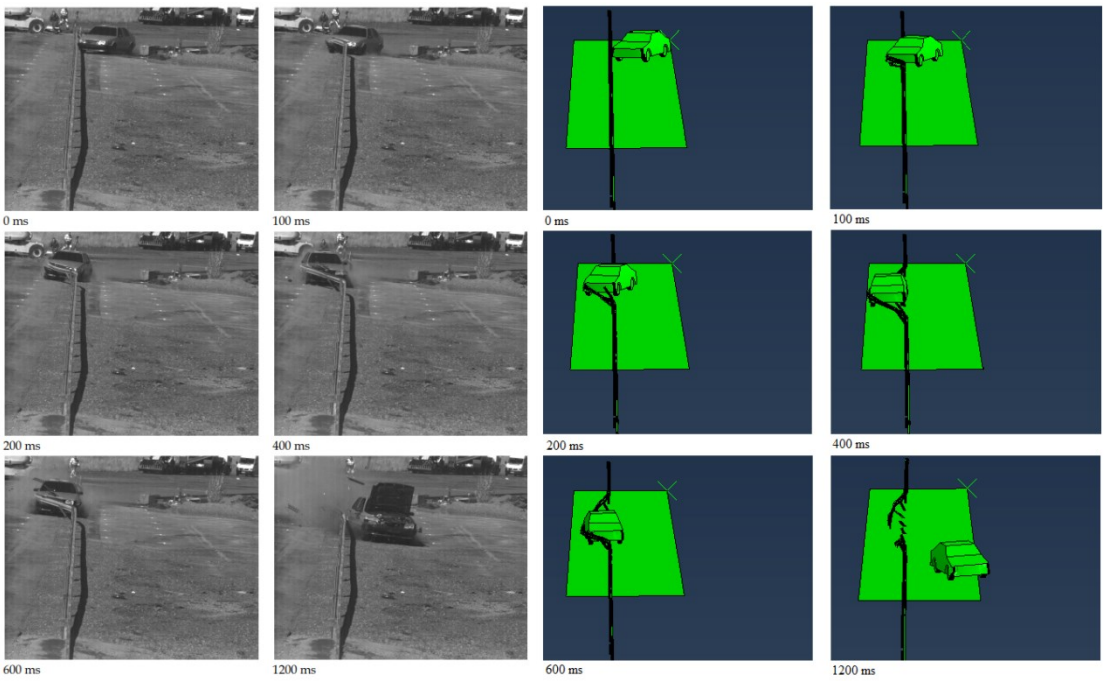

Figure 30. Periodic phots of the full-scale test and simulation of TB 32 test with sigma posts.

5.8 Model changes for new barrier assembly

The model has to be modified slightly for the development and optimization of the new barrier assembly. This is due to change in the material of the posts and rails, change of the rail assembly and change in the test setup.

The new barrier is to be manufactured out of different materials than the materials used in the tests the simulation model is based on. SSAB provided detailed properties of the new materials.

The rail used in the new barrier assembly is designed to attach directly to the previous rail. This eliminates the need for rail extension pieces. There is no need for a completely new model of the rail as the existing one can be modified to represent the new rail. The old rail and rail extension piece are trimmed and then joined together with a tie connection. This is presented in figure 31.

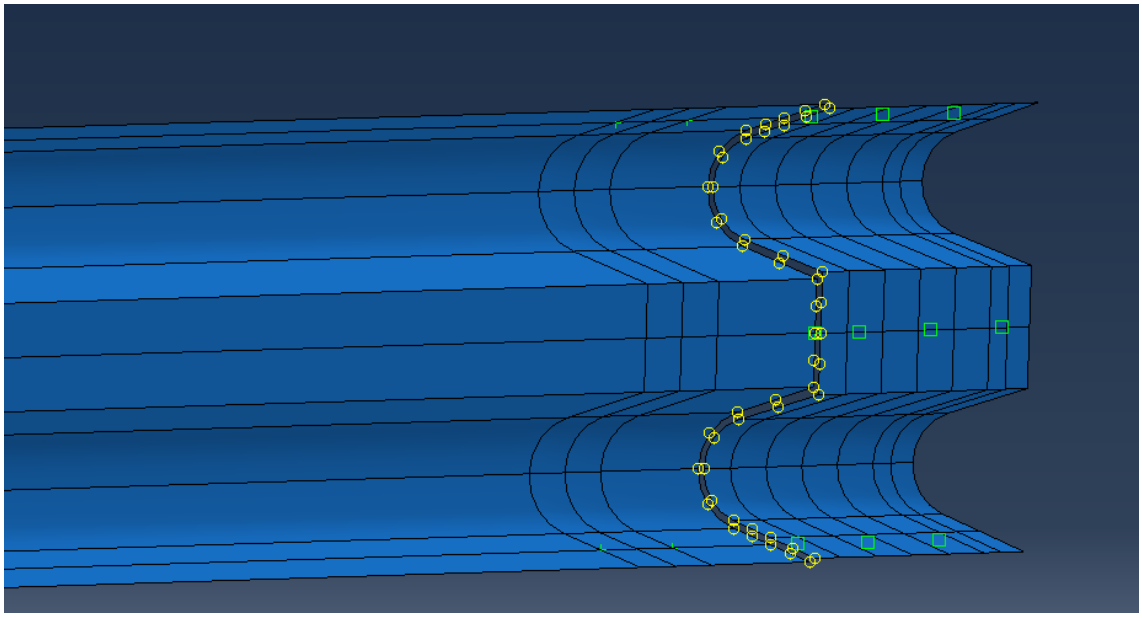

Figure 31. Connection of trimmed old rail and rail extension piece to form the new rail.

The test to be performed on the new barrier assembly is setup slightly differently than the full-scale tests the model was based on. The barrier is installed without the ascending and descending rails at the beginning and end. Instead the ends of the rail assembly are fixed with a tensioned cable. To take this change into account the model is changed slightly. The ascending and descending rails are removed and the barrier is instead fixed rigidly from both ends. Fixing the ends of barrier with cables more accurately represents a continuous rail.

6 IMPLEMENTATION OF OPTIMIZATION

As mentioned in chapter 3.3 the optimization method used is pattern-search method. Dakota offers several pattern search algorithms. Coliny_pattern_search, part of the SCOLIB optimizer package, is used for the optimization of the posts dimensions. SCOLIB is developed by Sandia National Laboratories. Coliny_pattern_search is a standard pattern search method that offsets the values of the design variables from the current iterate to find an improved point in the design space. If the first round of iterations doesn't find an improvement the offset is reduced. (Adams et al. 2018b.)

6.1 Objective and constraint functions

The function to be minimized is set up to be the dynamic deflection of the TB 32 simulation. Achieving a low dynamic deflection is beneficial for a barrier as it can then be graded with a low working width class and can be used for more demanding section of the road.

Achieving a small working width would be very easy by simply making the posts very stiff. However, this would make the impact severity levels very high. The main limiting factor for reducing the working width is the acceleration severity of the impact for the smaller TB 11 car. The lowest impact severity level A requires ASI to be less than 1 and THIV to be less than 33 km/h. ASI is easier to implement into the optimization code so the ASI of TB 11 simulation is set as the constraint function. The model has given consistently higher ASI in TB 11 simulations than recorded during the full-scale tests.

6.2 Design variables and constraints

Design variables are all related to the dimensions of the new posts profile. The new posts profile is slightly different than the ones used in the previous crash tests. The design variables are the height of the posts profile H, its width W and the length of the flange L.

The dimensions of the profile are constrained by the manufacturability of the profile and minimum length of an element to achieve decently long time increments and short run times. Design variables and their lower and upper bounds are presented in table 11.

Table 11. Design variables.

Design variables	Lower and upper bounds
H	$H_{min} \leq H \leq H_{max}$
W	$W_{min} \leq W \leq W_{max}$
L	$L_{min} \leq L \leq L_{max}$

With the objective function, constraint function and design variables and their bounds determined the optimization problem can be written in the standard form as follows:

$$\begin{aligned} &\text{minimize:} && f(\boldsymbol{x}) \\ & && \boldsymbol{x} = (\mathrm{W}, \mathrm{H}, \mathrm{L})^T \\ &\text{subject to:} && g(\boldsymbol{x}) \leq \mathrm{ASI}_{max} \\ & && \boldsymbol{x}_L \leq \boldsymbol{x} \leq \boldsymbol{x}_U \\ & && \boldsymbol{x}_L = (\mathrm{W}_{\min}, \mathrm{H}_{\min}, \mathrm{L}_{\min})^T \\ & && \boldsymbol{x}_U = (\mathrm{W}_{\max}, \mathrm{H}_{\max}, \mathrm{L}_{\max})^T, \end{aligned} \tag{21}$$

where f(**x**) is the dynamic deflection of TB 32 simulation, g(**x**) is the ASI of TB 11 simulation and vector **x** contains the design variables W, H, L, $\mathbf{x}_L$ contains the lower bounds for the design variable and $\mathbf{x}_U$ contain the upper bounds for the design variables.

6.3 Dakota setup

The optimization is set up as described earlier in figure 3. Dakota writes the design variables W, H and L into the parameter file. The coordinates of the nodes of the new post are then modified to match the dimensions of W, H and L. This is done by a template processing tool called dprepro that comes packaged with Dakota. The coordinates of the nodes of the new post are expressed as functions of W, H and L and written as template expressions delimited by "{}" inside the input file for Abaqus. Dprepro replaces template expressions inside the Abaqus input file with the correct coordinates of the nodes.

Once the input file is ready both TB 32 and TB 11 simulations are executed. A python script retrieves the dynamic deflection from the TB 32 output file and calculates ASI from the TB 11 output file and writes a Dakota results file containing both. The results file is read by Dakota. This is then repeated until satisfactory convergence is reached. The optimization is determined to have satisfactory convergence as the steps the pattern search takes have reduced to be less than 1 mm. The typical manufacturing tolerance for the dimensions W, H and L is 1 mm and it doesn't make sense to optimize the dimensions further.

Constraint function is handled as a penalty function. A constraint penalty set by user times the sum of the squares of the constraint violations is added to the objective function (Adams et al. 2018b). The constraint penalty is set to 20000 for the optimization of the post. This would mean a 0.01 violation of the ASI constraint function would increase the objective function by $0.01^2 * 20000 = 2$ mm.

7 RESULTS

The optimization ran for 6 iterations which add up to total of 32 evaluations of the objective function. Simulation of a single evaluation took approximately 2 hours so the total run time for the optimization process was approximately 64 hours. The results for the optimization run are presented in table 12. The results and the dimensions are presented as percentage of the dimensions and results of the initial run. Best results were achieved at evaluation number 23 with 99.4 % TB 32 dynamic deflection and 97.1 % TB 11 ASI compared to the evaluation 1. Dimensions for the optimal design are 101.5 % of the initial W dimension, 100 % of the initial L dimension and 95.5 % of the initial H dimension. Periodic pictures of the trajectory of the TB 32 simulation are presented in figure 32 and of the TB 11 simulation in figure 33. The cars leave the rail within the exit-box described in chapter 4.2.4.

Table 12. Optimization function evaluations.

Evaluation No.	Iteration	W	L	H	Dynamic deflection	ASI
1	0	100.0	100.0	100.0	100.0	100.0
2	1	106.0	100.0	100.0	97.5	102.4
3	1	100.0	137.2	100.0	97.4	101.0
4	1	100.0	100.0	103.0	98.3	102.0
5	1	94.0	100.0	100.0	101.4	97.4
6	1	100.0	62.8	100.0	100.6	98.9
7	1	100.0	100.0	97.0	99.8	97.8
8	2	106.0	100.0	97.0	98.3	100.3
9	2	100.0	137.2	97.0	99.0	98.8
10	2	94.0	100.0	97.0	101.2	95.4
11	2	100.0	62.8	97.0	101.4	96.6
12	2	100.0	100.0	94.0	100.6	95.5
13	3	103.0	100.0	97.0	99.8	99.1
14	3	100.0	118.6	97.0	100.2	98.3
15	3	100.0	100.0	98.5	100.5	98.9
16	3	97.0	100.0	97.0	101.6	96.2
17	3	100.0	81.4	97.0	100.6	97.1
18	3	100.0	100.0	95.5	100.0	96.8
19	4	103.0	100.0	95.5	99.8	98.1
20	4	100.0	118.6	95.5	100.1	97.3
21	4	97.0	100.0	95.5	100.9	95.3
22	4	100.0	81.4	95.5	100.4	96.2
23	5	101.5	100.0	95.5	99.4	97.1
24	5	100.0	109.3	95.5	99.8	97.1
25	5	100.0	100.0	96.3	99.9	97.3
26	5	98.5	100.0	95.5	100.9	96.0
27	5	100.0	90.7	95.5	100.2	96.3
28	5	100.0	100.0	94.8	100.1	96.1
29	6	101.5	109.3	95.5	101.1	97.6
30	6	101.5	100.0	96.3	100.7	98.0
31	6	101.5	90.7	95.5	100.9	97.1
32	6	101.5	100.0	94.8	99.7	97.0

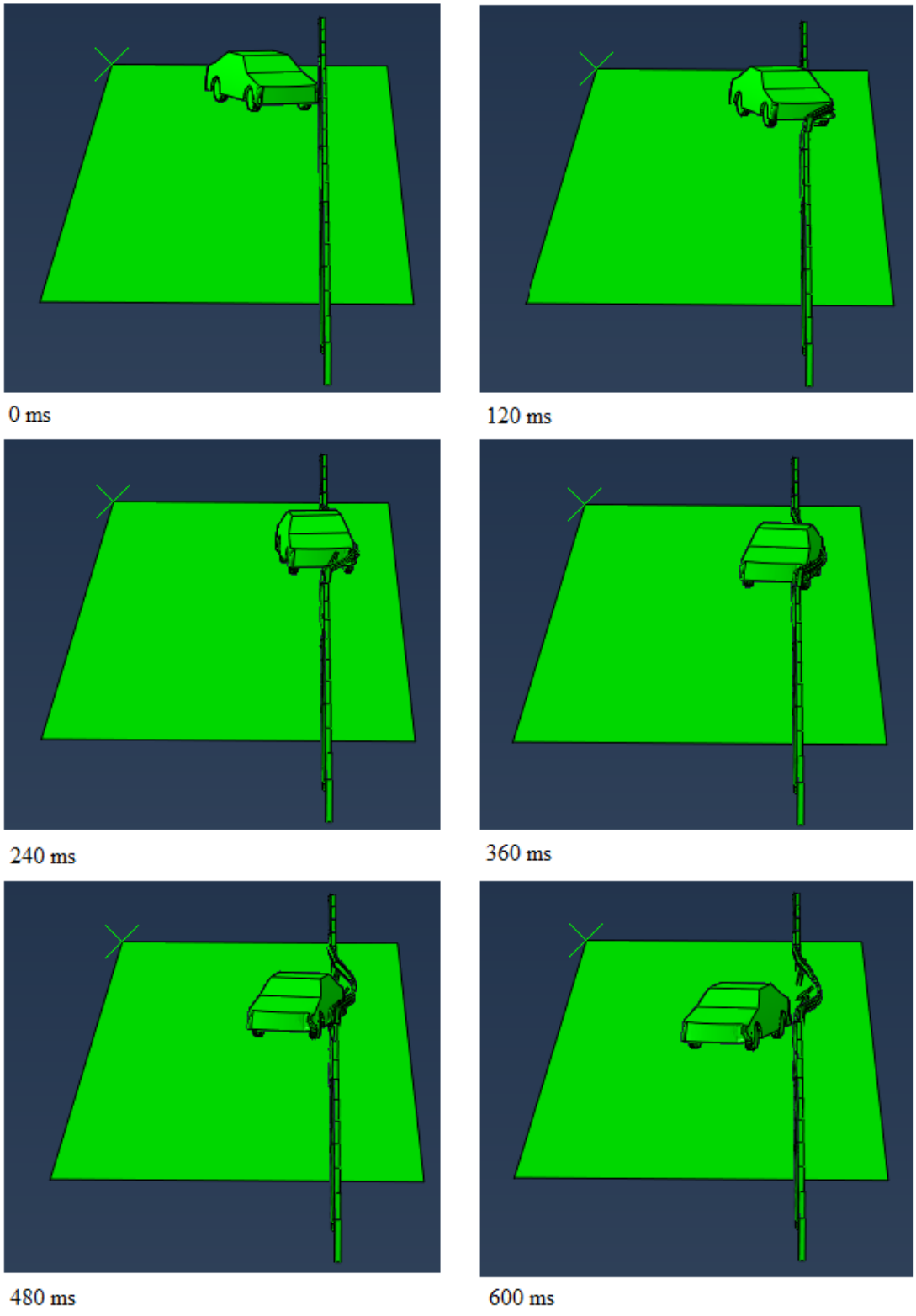

Figure 32. Periodic pictures of the trajectory of TB 32 car.

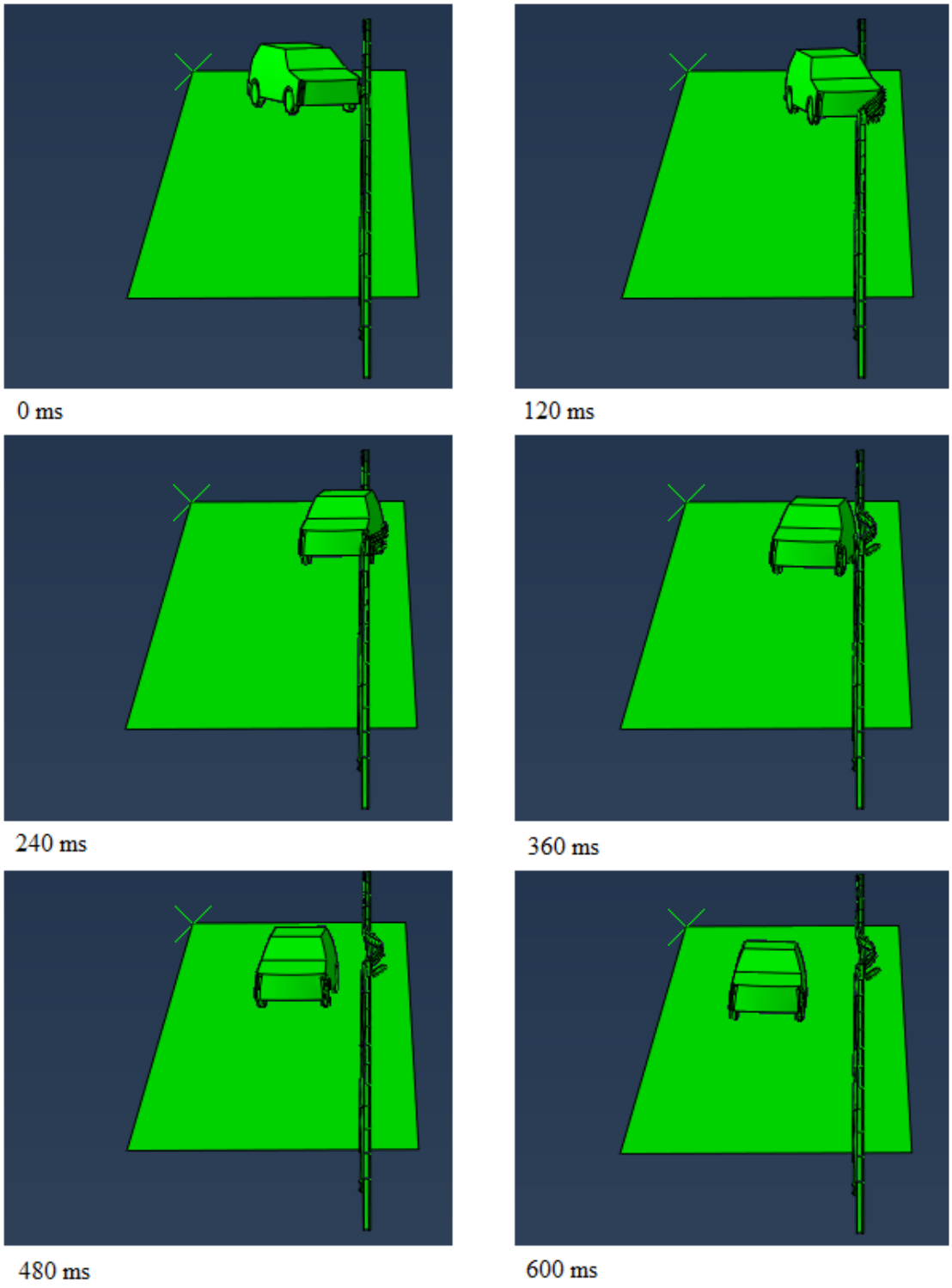

Figure 33. Periodic pictures of the trajectory of TB 11 car.

The performance of the barrier does not increase dramatically during the optimization process. Constraining ASI even higher would lead to lower dynamic deflection but this would leave little room for error when committing to a full scale test. Further developing and increasing the accuracy of the model, especially the accuracy of TB 11 simulation, could be considered. Developing the model further does have some drawbacks though.

Full scale test results with the effects of the change in the test setup described in chapter 5.8 are not available to be used in this thesis. Developing the model further without results from such a test might prove unnecessary work as the model likely has to be modified regardless after running the full-scale tests with the new test setup.

8 CONCLUSIONS

A sufficiently accurate simulation model of the crash test was successfully created. The model can be used to evaluate the performance of safety barrier still in development. Even though the models of the cars were very simplified the models behaved visually similarly to full-scale tests. However, running the simulations with a more detailed model of the cars, if such become available, is worth consideration to see if the accuracy improves. Using a more detailed car could however be more computationally expensive and thus increase time the optimization takes to converge.

The optimization results indicate that pattern search optimization methods or derivative free optimization methods in general are a viable solution to optimizing the dimensions of a roadside barrier or any structure simulated with explicit method. The implementation of the optimization process was fairly simple. The way Dakota handles input and output files couples well with Abaqus input files. The ease of implementation is a vital thing to consider when selecting the optimization software and method as the implementation can take a major part of the overall development time. The use of optimization can significantly reduce the time the designer has to use to iterate trough different designs. The usefulness of optimization would be even more apparent if the time required for each function evaluation was smaller. Adequate computational resources have to be available so that the computational time remains reasonable. Care must also be put into making the model as efficient as possible and selecting a suitable optimization method.

The variance in the results does complicate the optimization process. It is likely that the pattern search method eventually gets stuck in a local minimum. Using a sufficiently large initial step is important to counter this. The use of a global derivative free optimization method could be considered, for example genetic algorithm. This would be suitable if there were significantly more computational resources available. Running evolutionary algorithm with the current resources convergence would likely take weeks or even months.

9 REFERENCES

Abaqus, 2017. Online documentation [Online document].

Adams, B.M., Bauman, L.E., Bohnhoff, W.J., Dalbey, K.R., Ebeida, M.S., Eddy, J.P., Eldred, M.S., Hough, P.D., Hu, K.T., Jakeman, J.D., Stephens, J.A., Swiler, L.P., Vigil, D.M., and Wildey, T.M., 2018a. Dakota, A Multilevel Parallel Object-Oriented Framework for Design Optimization, Parameter Estimation, Uncertainty Quantification, and Sensitivity Analysis: Version 6.8 User's Manual [online document]. New Mexico: Sandia National Laboratories. SAND2014-4633. Available: https://dakota.sandia.gov/content/manuals. [cited 3.1.2019]. 386 p.

Adams, B.M., Bauman, L.E., Bohnhoff, W.J., Dalbey, K.R., Ebeida, M.S., Eddy, J.P., Eldred, M.S., Hough, P.D., Hu, K.T., Jakeman, J.D., Stephens, J.A., Swiler, L.P., Vigil, D.M., and Wildey, T.M., 2018b. Dakota Reference Manual 6.8 [online document]. New Mexico: Sandia National Laboratories. Available: https://dakota.sandia.gov//sites/default/files/docs/6.8/html-ref/index.html. [cited 7.1.2019].

Antoniou, A. & Lu, W. 2007. Practical Optimization: Algorithms and Engineering Applications. Springer, 674 p. ISBN 1441943838

Belytschko, T., Liu, W. & Moran, B. 2014. Nonlinear finite elements for continua and structures. Chichester: John Wiley & Sons, Inc, 650 p. ISBN 9781118632703

Dassault systèmes, 2009. Crashworthiness Analysis with Abaqus [Online document]. 614 p.

SFS-EN 1317-1, 2010. Road restraint systems. Part 1: Terminology and general criteria for test methods. Suomen standardoimisliitto SFS: 27 + 9 p.

SFS-EN 1317-2, 2010. Road restraint systems. Part 2: Performance classes, impact test acceptance criteria and test methods for safety barriers including vehicle parapets. Suomen standardoimisliitto SFS: 21 + 7 p.

Koziel, S. & Yang, X-S. 2011. Studies in Computational Intelligence, Volume 356: Computational Optimization, Methods and Algorithms. Berlin Heidelberg: Springer-Verlag, 292 p. ISBN 978-3-642-20858-4

Naresh Kumar, G., Ikram, M., Sarkar, A.K. & Talole, S.E. 2018. Hypersonic flight vehicle trajectory optimization using pattern search algorithm. Optimization and Engineering, 19 (1), p. 125-161.

National Academies of Sciences, Engineering, and Medicine 2011. Procedures for Verification and Validation of Computer Simulations Used for Roadside Safety Applications. Washington, DC: The National Academies Press. Available: https://doi.org/10.17226/17647 [cited 3.1.2018]. 560 p.

Rao, S.S. 2009. Engineering Optimization: Theory and Practice. John Wiley & Sons, Inc, 840 p. ISBN 9780470183526

Ren, Z. & Vesenjak, M. 2005. Computational and experimental crash analysis of the road safety barrier. Engineering Failure Analysis, 12 (6), p. 963-973.

Shan, S. & Wang, G. G. 2010. Survey of modelling and optimization strategies to solve high-dimensional design problems with computationally-expensive black-box functions. Structural and Multidisciplinary Optimization, 41 (2), p. 219-241.

Teng, T-L., Liang, C-C. & Tran, T-T. 2016. Development and validation of a finite element model for road safety barrier impact tests. Simulation: Transactions of the Society for Modeling and Simulation International, 92 (6), p. 565-578.

Wu, S. & Lei, G. 2012. Introduction to the Explicit Finite Element Method for Nonlinear Transient Dynamics. Hoboken: John Wiley & Sons, Inc, 353 p. ISBN 9780470572375